Vegetation and peat accumulation steer Holocene tidal–fluvial basin filling and overbank sedimentation along the Old Rhine River, The Netherlands

HARM JAN PIERIK*,1 (iD), JELLE I. M. MOREE*,2, KARIANNE M. VAN DER WERF*,3,
LONNEKE ROELOFS* (iD), MARCIO BOECHAT ALBERNAZ*,4, ANTOINE WILBERS†,
BERT VAN DER VALK‡, MARIEKE VAN DINTER§, WIM Z. HOEK* (iD),
TJALLING DE HAAS* (iD) and MAARTEN G. KLEINHANS* (iD)
*Department of Physical Geography, Faculty of Geosciences, Utrecht University, P.O. Box 80.115,
Utrecht, 3508 TC, The Netherlands (E-mail: hj.pierik@cultureelerfgoed.nl)
†IDDS Archeologie, 's-Gravendijckseweg 37, Noordwijk, 2201 CZ, The Netherlands
‡Department Applied Morphodynamics, Deltares, Boussinesqweg 1, Delft, 2629 HV, The Netherlands
§ADC Archeoprojecten, Nijverheidsweg-Noord 114, Amersfoort, 3812 PN, The Netherlands

ABSTRACT

In the transformation from tidal systems to freshwater coastal landscapes, plants act as eco-engineering species that reduce hydrodynamics and trap sediment, but nature and timing of the mechanisms of land creation along estuaries remains unclear. This article focuses on the Old Rhine estuary (The Netherlands) to show the importance of vegetation in coastal landscape evolution, predominantly regarding tidal basin filling and overbank morphology. This estuary hosted the main outflow channel of the river Rhine between *ca* 6500 to 2000 cal BP, and was constrained by peat during most of its existence. This study reconstructs its geological evolution, by correlating newly integrated geological data and new field records to varying conditions. Numerical modelling was performed to test the inferred mechanisms. It was found that floodbasin vegetation and resulting organic accumulation strongly accelerated back-barrier infill, by minimizing tidal influence. After tidal and wave transport had already sufficiently filled the back-barrier basin, reed rapidly expanded from its edges under brackish conditions, as shown by diatom analysis and datings. Reed growth provided a positive infilling feedback by reducing tidal flow and tidal prism, accelerating basin infilling. New radiocarbon dates show that large-scale crevassing along the Old Rhine River – driven by tidal backwater effect – only started as nutrient-rich river water transformed the floodbasin into an Alder carr in a next phase of estuary evolution. Such less dense vegetation promotes crevassing as sediments are more easily transported into the floodbasin. As river discharge increased and estuary mouth infilling progressed, crevasse activity diminished around 3800 to 3000 cal BP, likely due to a reduced tidal backwater effect. The insights from this data-rich Holocene study showcase the dominant role that

[1]Present address: Landscape Department, Cultural Heritage Agency of The Netherlands, Smallepad 5, Amersfoort, 3811 MG, The Netherlands
[2]Present address: Department of Environmental Sciences, Wageningen University, Droevendaalsesteeg 3, Wageningen, 6708 PB, The Netherlands
[3]Present address: Witteveen+Bos, Leeuwenbrug 8, Deventer, 7411 TJ, The Netherlands
[4]Present address: Waterproof BV, IJsselmeerdijk 2, Lelystad, 8221 RC, The Netherlands

1

vegetation may have in the long-term evolution of coastal wetlands. It provides clues for effective use of vegetation in vulnerable wetland landscapes to steer sedimentation patterns to strategically adapt to rising water levels.

Keywords Estuary, Holocene, infilling, peat accumulation, vegetation.

INTRODUCTION

As sea-level rise decelerated during the middle Holocene, many estuaries with abundant sediment supply started to fill in (Roy *et al.*, 1980; Nichol, 1991; Van der Spek, 1995; Umitsu *et al.*, 2001; Vos, 2015; Clement *et al.*, 2017; De Haas *et al.*, 2018, 2019). The degree of estuary infilling depends on a complex interaction between sediment supply, accommodation (also referred to as accommodation space) and hydrodynamics. The role of vegetation in estuary evolution is increasingly becoming clear and therefore incorporated to study long-term estuary evolution (Coco *et al.*, 2013; De Haas *et al.*, 2018; Lokhorst *et al.*, 2018; McMahon & Davies, 2018; Brückner *et al.*, 2019; Boechat Albernaz *et al.*, 2020). Vegetation is known to play an important role in sedimentation processes and spatial patterns in coastal wetlands (Redfield, 1965). It affects hydrodynamics and steers spatial sedimentation patterns, for example in saltmarshes (D'Alpaos *et al.*, 2006; Temmerman *et al.*, 2007; Fagherazzi *et al.*, 2012; Schepers *et al.*, 2020) or in reed margins along tidal basins (Rooth & Stevenson, 2000). Its effects on the scale of an entire estuary is, however, less well studied.

Vegetation may accumulate into peat; it then fills accommodation space, aiding to keep up with sea-level rise where sediment supply alone may be insufficient (Bos *et al.*, 2012; Vos, 2015). As such, peat may be a strong contributor to terrestrialization in tidal environments (Den Held *et al.*, 1992). The local scale effects of peat on sedimentation patterns are generally well-known. These include resistance to lateral erosion, confining channels and levées (Smith & Pérez-Arlucea, 2004; Makaske *et al.*, 2007), as well as providing local accommodation and increasing flood risk due to being prone to compaction (Long *et al.*, 2006; Van Asselen *et al.*, 2009; Pierik *et al.*, 2017). Despite these known local effects, peat accumulation on estuary and tidal basin scale is often implicitly regarded to follow coastal plain and estuary evolution rather than being seen as an agent contributing to it. In the coastal plain around the North Sea, for example, mid-

Holocene peat accumulation is often associated with barrier closure as a prerequisite for back-barrier freshening (Baeteman, 1999 – Belgian coastal plain; Allen, 2000 – Gwent, UK; Beets & Van der Spek, 2000 – The Netherlands; Long *et al.*, 2000; Sawai *et al.*, 2002 – Hokkaido; Deforce, 2011 – Scheldt, Belgium/The Netherlands; Wartenberg *et al.*, 2013 – Jade Germany; Brew *et al.*, 2015; Hamilton *et al.*, 2019 – UK). Given the importance of the earlier mentioned local peat effects, however, deltas and coastal plains must be strongly co-shaped by vegetation and peat, besides being the result of morphodynamic evolution. But to what extent are vegetation and peat formation driving factors in back-basin infilling and how important are they for the evolution of an estuary as a whole?

A portion of the infilled back-barrier basin along the Old Rhine consists of natural levée and crevasse deposits (together: overbank deposits), which formed under flood water levels (e.g. Brierley *et al.*, 1997; Bos & Stouthamer, 2011). Their shape, size and distribution strongly varies as a function of sediment supply and flood regime (Hudson & Heitmuller, 2003; Adams *et al.*, 2004; Millard *et al.*, 2017; Boechat Albernaz *et al.*, 2020). Besides these external conditions, the nature of the receiving flood basin, for example, interaction with vegetation (Pierik *et al.*, 2017a,b; Kleinhans *et al.*, 2018; Nienhuis *et al.*, 2018; Boechat Albernaz *et al.*, 2020) and compaction prone substrate (Van Asselen, 2011), are increasingly acknowledged to affect overbank morphology. How variation in levée and crevasse sedimentation along tidal rivers can be explained in terms of these factors combined remains unclear.

This paper deciphers the role of peat growth and floodbasin vegetation in the Holocene infilling of the Old Rhine estuary in The Netherlands (active *ca* 6500–1000 cal BP). The Old Rhine was the largest Rhine branch in the lower Rhine-Meuse delta, situated in a 60 km wide coastal plain (Fig. 1). This coastal plain is well-preserved and much data on its geological evolution and boundary conditions are available to unravel these complex interactions. This paper

builds upon a recent synthesis of the Holocene evolution of the Old Rhine mouth by De Haas *et al.* (2019). New borehole data, dates and diatom analyses (examples in Figs 2 to 4) are combined with existing geological data and key archaeological studies to reconstruct phases in basin terrestrialization and estuary evolution. These developments are then correlated to changing fluvial discharge, tides, sediment supply and floodbasin vegetation. The emerged physical processes and mechanisms inferred from the geological record were further tested in Delft3D morphodynamics numerical models.

THE OLD RHINE ESTUARY: SETTING AND EVOLUTION

This section briefly summarizes the setting and evolution of the study area, partly based on the review by De Haas *et al.* (2019).

Geographical and geological setting

The Old Rhine River was active as the main distributary course of the Rhine between *ca* 6500 and 2000 cal BP. It was positioned in the northwestern part of the Rhine-Meuse delta, flowing through the Holocene back-barrier towards the North Sea (Beets & Van der Spek, 2000; Berendsen & Stouthamer, 2000; De Haas *et al.*, 2019). The Holocene back-barrier wedge formed after post-glacial sea-level rise, its thickness ranges from *ca* 10 m near the present coast to 3 m near Utrecht (*ca* 50 km upstream). The upper metres predominantly consist of peat, a remnant of an exceptionally wide coastal peat swamp along the North Sea. This swamp formed on the low gradient pre-Holocene sandy substrate, allowing waves to build barriers relatively seaward (Beets & Van der Spek, 2000; De Haas *et al.*, 2018). Behind these protecting elements, tidal energy, water depth and salinity eventually became low enough for reed to grow and peat to accumulate
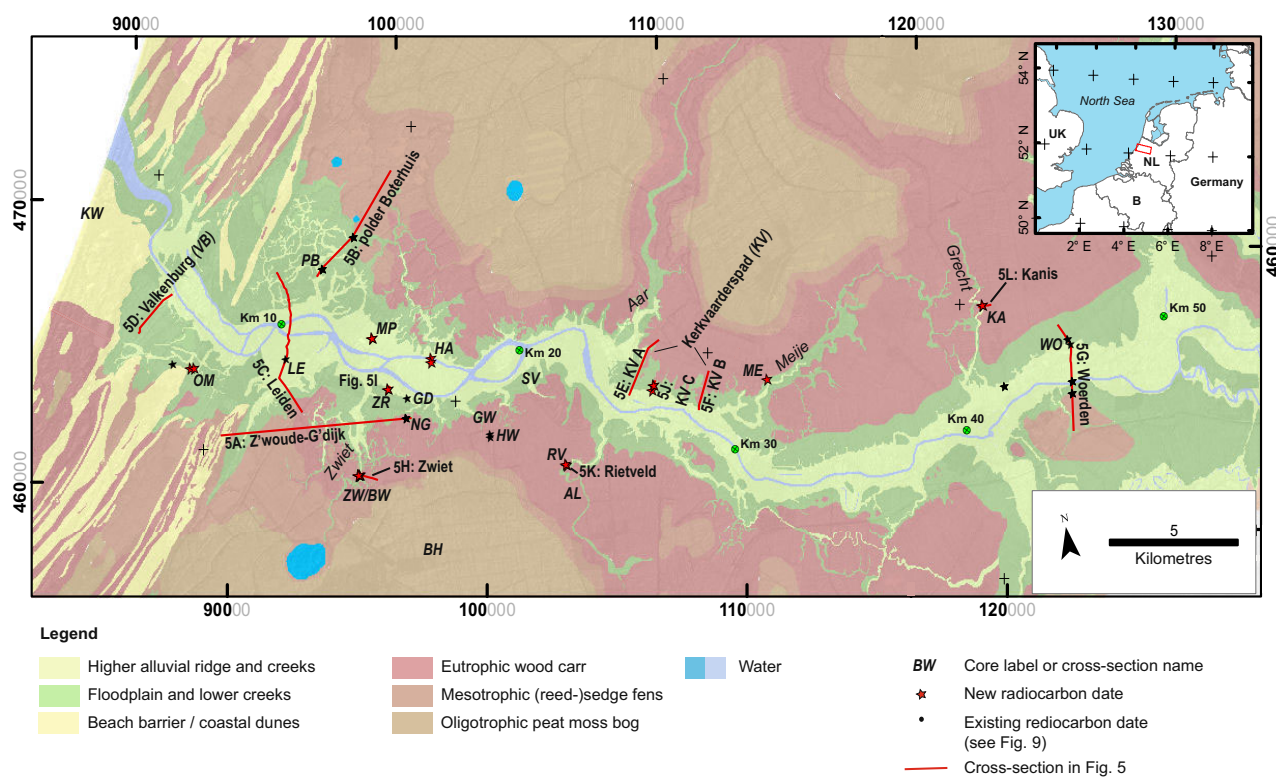

Fig. 1. Location and setting of the study area. Background palaeogeographical reconstruction for Roman Age (*ca* 1850 cal BP) as reconstructed by Van Dinter (2013). Crevasses into the peatlands have been based on LiDAR/soil maps. As significant peat compaction and oxidation has taken place since the Middle Ages, their Roman Age extent may be overestimated here. Indicated kilometre (Km) points are measured relative to the current coast in upstream direction along the Old Rhine channel belt axis. Locations of the cross-sections in Fig. 5 and dated sites in Figs 3, 4 and 9 are indicated.
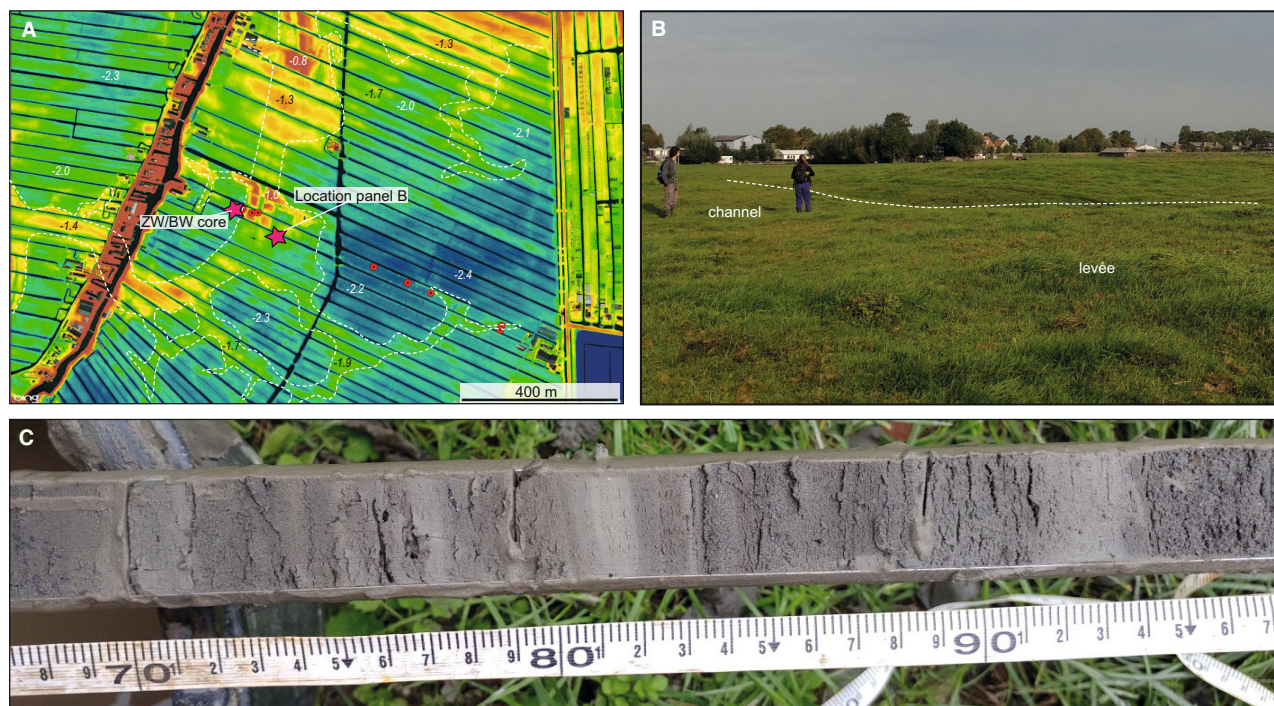
© 2022 The Authors. *Sedimentology* published by John Wiley & Sons Ltd on behalf of International Association of Sedimentologists., *Sedimentology*

Fig. 2. Setting and core of the Zwiet creek (*ZW* = Broekweg location *BW*). For location, see Fig. 1. (A) LiDAR image of the creek shows inversion ridges in the peatland; (B) creek relief in the field looking north-west, photograph taken from levée top, geologists standing in the channel (*ca* 1.8 m tall); (C) tidal bundling below 170 cm below surface level in levée of the Zwiet creek (borehole 201 801 037 in western levée in Fig. 5H).

(accounting for *ca* 5% of the volume of the current Holocene wedge – Beets & Van der Spek, 2000). Next to eutrophic reed swamps, Alder/Willow carrs, mesotrophic sedge fens and oligotrophic peat moss bogs formed in the coastal plain, depending on the trophic and hydrological conditions (Pons, 1992; Bos *et al.*, 2012).

The coastline approached the present-day South Holland coast around 8500 cal BP (Hijma & Cohen, 2011). From then onwards, wave-driven mobilization transported sand onshore in the study area, but it was not until *ca* 6000 cal BP, that marine and fluvial sedimentation could keep up with the accommodation generated by sea-level rise (Beets *et al.*, 1992; Beets & Van der Spek, 2000). Wave-driven sediment supply led to beach-barrier formation and sedimentation in the back-barrier tidal basins, and subsequent progressive closure of tidal inlets. The back-barrier basins were flanked by reed marshes and their deposits consist of sand, topped by blue grey silty clays. Often (younger) reed roots are found from overlying reed peat beds (Bosch & Pruissers, 1979; Van der Valk, 1995). Based on radiocarbon dates of shells, the tidal channels in

the back barrier basin reached their maximal size before 6400 and closed around 6100 cal BP (Van der Valk, 1995; Cleveringa, 2000; Hijma *et al.*, 2009). The largest tidal inlet, the Rijswijk–Zoetermeer system reached its maximum size between *ca* 6800 and 6400 cal BP and closed around 6100 cal BP. The smaller Voorschoten tidal system was largest after 6400 cal BP and sandy deposition of the nearby Stompwijk tidal system also ended around 6100 cal BP (Fig. 6). This closing trend is reflected in *in situ* mollusc fauna at site *BH* (Fig. 1) that indicate salinity decrease from 10–15‰ to 8–10‰ (parts per thousand ~ grams of salt per kilogram of water) for the top metre, indicating very shallow brackish water (Raven & Kuijper, 1981).

Around 6500 cal BP, the Rhine branch avulsed towards the north, where it would remain for several millennia (Hijma & Cohen, 2011; Cohen *et al.*, 2012), using the pathway of an old tidal inlet (De Haas *et al.*, 2019). Freshening due to barrier closure and river presence is generally assumed to have resulted in extensive peat formation from 5500 to 5300 cal BP onwards (Hijma *et al.*, 2009; Vos, 2015), and hence peat

formation has so far mainly been considered a consequence of morphological evolution rather than contributing to it. Fed by freshwater from rivers and rain, *Phragmites* and Alder marshes expanded in the back-barrier area, locally evolving into ombrotrophic elevated bogs (Pons *et al.*, 1963; Pons, 1992; Vos, 2015). During floods, fine sediments from rivers and the sea could still reach the fens in the Rhine-Meuse delta. As a result, *Phragmites* peat here typically contains 25 to 65% of clay and silt admixed, while Alder peat generally contains 17 to 70% of clastic material (Bos *et al.*, 2012). Meanwhile at the coast, the beach barriers and dunes gradually accreted seaward until *ca* 2000 cal BP, forming a 9 km wide beach-barrier complex (Roep *et al.*, 1991; Van der Valk, 1995; Cleveringa, 2000). In its final mature stage, the river formed the northern border of the Roman Empire, the *Limes*, in the first to third century AD (Van Dinter, 2013). The *Limes* was granted the status of World Heritage by UNESCO in 2021. Afterwards, the river discharge gradually diminished after upstream avulsions had occurred, until the river was dammed upstream at Wijk bij Duurstede in AD 1122.

During the time when the Old Rhine was active, levées, crevasses and floodbasin deposits were formed in multiple phases, separated by peat layers. The thick peat surrounding the Old Rhine channel belt caused the position of the river to remain relatively fixed, limiting lateral migration (Makaske, 1998; Van Asselen, 2011). Furthermore, the peat layers enabled the formation of thick natural levées due to high compaction rates of the peat below them (Van Asselen, 2011). Between kilometre 10 and 50 (Fig. 1), long crevasse splays expand into the peat lands (Berendsen, 1982; Van Dinter, 2013). These likely formed navigation corridors through otherwise inaccessible peatlands in and before Roman times, but their exact age is unknown. Trends in their orientation, length and abundance towards the mouth suggest a degree of tidal influence (Van Dinter, 2013). Upstream of the characteristic estuary backwater length, crevasses are more scarce and much shorter (De Haas *et al.*, 2019). Apart from these morphological observations, their age of activity and formative factors have not been well-assessed.

Upstream boundary conditions

The upstream boundary conditions, discharge, sediment load and flood frequency along the Old Rhine are relatively well-known. The present-day Rhine has an average discharge of 2260 m^3/s and discharge is estimated to have varied <10% during the Holocene (Erkens & Cohen, 2009; Stouthamer *et al.*, 2011). Over the Holocene, the frequency of large floods from the Rhine river has varied considerably due to climate change and growing human impact (Toonen *et al.*, 2013, 2017; Jansma, 2020). Before *ca* 3800 cal BP, a small portion of Rhine discharge was routed towards small distributaries into the peatlands in the western Rhine-Meuse delta, south of our study area (Makaske *et al.*, 2007; Cohen *et al.*, 2012). These distributaries silted up after *ca* 3800 cal BP leading more discharge towards the Old Rhine (Stouthamer & Berendsen, 2001). Fine sediment supply by the Rhine increased by *ca* 60% after *ca* 3000 cal BP due to deforestation in the Rhine catchment (Hoffmann *et al.*, 2007; Erkens & Cohen, 2009). Increased flood frequency and fine sediment supply most likely led to increased deposition of fines and more frequent avulsions, especially in the last 2800 years, when the Old Rhine was gradually abandoned (Stouthamer *et al.*, 2011). Around 2800 cal BP the Rhine partly avulsed into the Oer-IJ (Bos *et al.*, 2009), followed by the Hollandse IJssel and Lek (Pierik *et al.*, 2018), and the Waal and Gelderse IJssel (Berendsen & Stouthamer, 2000; Cohen *et al.*, 2009; Kleinhans *et al.*, 2011). This led to a stepwise decrease in river discharge and led to the formation of an underfit channel, which subsequently narrowed down (Van Dinter *et al.*, 2017; De Haas *et al.*, 2019).

Downstream boundary conditions

The post-Last Glacial Maximum sea-level rise progressively slowed down from *ca* 11 mm/yr around 8200 cal BP to a rate of 1 to 2 mm/yr over the last 2000 years (Hijma & Cohen, 2019). In the lifetime of the Old Rhine, sea level rose by *ca* 5 m. This provided accommodation for peat accumulation and preservation of overbank deposits (Koster *et al.*, 2016). The tidal range at the estuary mouth has been stable around 1.5 m and the significant wave height gradually increased from *ca* 0.8 m around 6000 cal BP to 1 m today (Van der Molen & De Swart, 2001a,b). From 6000 cal BP onwards, beach barriers gradually closed. Around the Old Rhine they accreted until *ca* 3000 cal BP resulting in a 10 km wide beach-barrier complex. Beach-barrier accretion caused the estuary mouth to shift seaward, most

likely decreasing tidal influence along the river. This effect was further enhanced as the estuary filled in and even more when the mouth shifted northward (De Haas *et al.*, 2019) as discharge decreased in the final stages of the Old Rhine. This paper reconstructs these phases of progressive infilling in more detail and links them to overbank phases along the river.

METHODS

To study the effect of vegetation and peat accumulation on back-barrier infilling and subsequent estuary evolution, a complementary approach of field data and numerical modelling was used. This approach reconstructed local floodbasin conditions, the downstream and upstream boundary conditions, and linked these to changes observed in the sedimentary record. The transition from tidal back-barrier clays to terrestrial peat was sampled, which is considered an expression of important landscape change. This interval was analyzed using diatoms. Additionally, the chronology of levée and crevasse activity in these peatlands was assessed as a potential indicator of changing estuary conditions. Their occurrence and their planform geometry were derived from existing datasets (e.g. Van Dinter, 2013), their stratigraphy was derived from borehole databases and local developer-funded archaeological studies. In addition, four crevasses, three natural levées, and two tidal-to-peat transitions were sampled and subsequently dated. Sampling sites were selected from upstream to downstream to assess the relative impact of fluvial and tidal boundary conditions.

In addition, two new reconstructions were made for the evolution of the mouth to better understand changes in downstream boundary conditions. This was done by updating existing reconstructions with new data from this study and from recent archaeological research (e.g. Blom & Roessingh, 2007; Tol & Jansen, 2012; Meijer *et al.*, 2020). Numerical modelling using Delft3D was performed (Deltares, 2017; Boechat Albernaz *et al.*, 2020) to test the hypotheses and mechanisms derived from the new geological reconstructions.

Field data and age estimates

For all field locations, levée and crevasse splay stratigraphy was studied based on multiple hand-cored boreholes. For every ten centimetres, lithology was described based on the Dutch classification scheme of De Bakker & Schelling (1966) and peat classification by Bos *et al.* (2012), clastics are presented here in the USDA classification scheme (Schoeneberger *et al.*, 1998; Soil Survey Staff, 2010). During the fieldwork, plant remains were identified visually, calcium content was determined using HCl (10%) and bedded structures were described. From the new and existing borehole data, lithological and geological cross-sections were made following, for example, Berendsen (1982) and Gouw & Erkens (2007).

Phases of overbank activity were dated at multiple locations along the Old Rhine. Both existing and newly obtained ^{14}C ages were used as well as archaeological finds (from the national ARCHIS database) on top of the crevasses and levées (cf. Berendsen, 1982; Törnqvist & Van Dijk, 1993; Pierik *et al.*, 2018). The top of the peat just below the overbank deposits was sampled as maximum ages (TPQ) of the beginning of overbank deposition. End phases were approximated by dating peat samples on top of overbank deposits (TAQ). Additionally, leaf samples in the top of the crevasse residual channel were used as dating material of final crevasse activity. The fieldwork sites were located as close as possible to the channel belt or the crevasse channel, where a gradual (i.e. a non-erosive stratigraphic) boundary was still observed between the peat and overlying clay. The best interval to select and date macrofossils from was found by using Loss-On-Ignition (LOI according to Heiri *et al.*, 2001). With this method, consecutive 1 cm intervals were sampled to measure mass percentage organic content to target the highest organic interval just below significant increase of clastics (i.e. the youngest peat below the levée or crevasse). Intervals below increasing clastic input were selected for terrestrial macrofossil sampling (Törnqvist & Van Dijk, 1993). All radiocarbon dates are reported in cal yr BP with a 1σ range, following the IntCal20 calibration curve of Reimer *et al.* (2020) in OxCal (Bronk Ramsey & Lee, 2013).

Environmental reconstruction using diatoms

To trace the terrestrialization process around the tidal clay–peat interval, core samples were taken at locations that would be representative of back-barrier area conditions around the time of basin closure. Where possible low energy

palaeo-environments were selected to ensure preservation of diatom valves in the substrate. One core was taken near the landward side of the former tidal basin, in proximity to fluvial influence and sampled in high resolution (*GW* – Figs 1 and 3). A second core was taken further seaward and further from the Old Rhine River, at a location that may have experienced large marine influence from the more southern Rijswijk–Zoetermeer inlet system (*BW* – Figs 1 and 4). The seaward core serves to substantiate the high resolution analysis of the landward core. The sample depths were chosen based on lithology, presence of *Phragmites* remnants and colour of the substrate. In the landward *GW* core, above the clay–peat contact, additional samples were taken at high resolution (1–2 cm intervals), to track changes in diatom assemblages during the terrestrialization process. Samples were prepared according to Renberg (1990). Valves were counted under a Leica DM LB2 light microscope (Leica Microsystems, Wetzlar, Germany) using 63× (times 1.5×) magnification and oil immersion. Per slide, *ca* 250 valves were counted, deemed sufficient for a statistically sound representation of the diatom assemblage (STOWA, 2014). Only diatoms with valves more than 70% intact were counted (cf. Batterbee *et al.*, 2001). Identification of non-freshwater species mainly relied upon the overview of Dutch diatom flora by Van der Werff & Huls (1974), for additional consulted studies see Appendix S1. The identified diatom species were classified into five salinity categories (Table 1) (details are provided in Van der Werf, 2020). Species that have a wider tolerance for salinity were assigned to their preferred or most commonly mentioned habitat conditions. Resting spores of *Chaetoceros* species were combined into one category (CRS), as identification to species level is not possible, and grouped under the Marine-category, because CRS do not occur in freshwater environments (Warnock *et al.*, 2018, and references therein). Diatoms for which identification to species level or specification of salinity conditions were inconclusive were grouped under unidentified/miscellaneous. Despite some small percentages of unidentified/miscellaneous diatoms, the trends in salinity conditions are strong.

Modelling overbank evolution

The effects of tidal–fluvial discharges and distinct vegetation typologies on the morphology inferred from the field data were tested using the morphodynamic model of Delft3D. The Delft3D model is widely used to simulate flow, sediment transport and morphology. The model accurately computes hydrodynamics of currents and waves, effects of vegetation on the hydrodynamics (Deltares, 2017), and resulting morphology with several options of sediment transport predictors (see Lesser *et al.*, 2004). The model solves the momentum and continuity equations for unsteady shallow-water flow in depth-averaged mode through the Navier–Stokes equation with hydrostatic pressure approximation (Deltares, 2017).

The isolated effects of varying tidal amplitudes, river discharge, flood magnitudes and the presence of dense (reeds) and sparse (wood) vegetation in tidal basins has been analyzed by Boechat Albernaz *et al.* (2020). Here, these simulations were expanded with three model scenarios, with boundary conditions that resemble different stages along the evolution of the Old Rhine after peat initiation (Table 2). The model results were used to enlighten the interpretation of our field data focused on the mechanisms behind levée and crevasse evolution.

An idealized estuary was designed consisting of an upstream river debouching into a floodbasin enclosed by barrier islands that communicates to the open coast through an inlet. Levées and crevasses could freely develop inside a floodbasin (of 12.5 km by 10 km). This floodbasin was connected to an upstream river boundary while the downstream end terminates in a coastal tidal domain. An initial channel was carved along the floodbasin to connect the upstream river to the coastal barrier. The initial channel dimensions followed the geometric relation of $Q = whu$ where Q is the river discharge in m^3/s; w the channel width; h the channel depth and u (depth averaged) flow velocity. This relation aimed for an initial flow velocity of 0.5 m/s and constant width-depth ratio of approximately 45. For example, a scenario with 700 m^3/s discharge consists of a channel 250 m wide and 5.5 m deep. The sediment transport predictor of Van Rijn (2007 I, II) was applied because it computes both bed and suspended load for multiple sediment fractions between mud and sand. Six sediment fractions were used, including clay, silt and four sand grain sizes, from which levées, crevasses and floodbasins could be built. The effect of floodbasin vegetation with high and low stem densities was simulated (based on Van Oorschot *et al.*, 2017; Brückner *et al.*, 2020). Note that our scenarios

only consider vegetation but not peat formation or its presence. Lastly, the bed composition was recorded in vertical layers of 10 cm resolution for each sediment fraction (van Kessel et al., 2012). This generates substrate composition and architecture that can be compared to the geological data.

In total, 61 scenarios were reanalyzed (see Boechat Albernaz et al., 2020), from which three were selected to resemble phases of the Old Rhine (Table 2). These scenarios resemble different environments that were present along the Old Rhine over its lifetime, as reconstructed in this paper. Two types of vegetation in the floodbasins and varying fluvial discharge were used. The evolution of unvegetated, less dense and very dense vegetation were assessed [models 40, 63 and 64 – see Boechat Albernaz et al., 2020], the latter two representing wood carrs and reed marshes, respectively. For the boundary conditions, different tidal ranges between 0.25 and 1.25 m were tested (also mimicking changes of the estuary mouth), and fluvial average discharges between 400 and 1500 m³/s and flooding regimes. From these scenarios, three were selected: (i) scenario 96 – with the transition from the marine-dominated environment with reed; (ii) scenario 74 – evolving to the situation when the tides diminished and Alder carr was dominant; and (iii) scenario 104 – the later stage when the fluvial discharges increased, also in the presence of Alder carr. More specific model details as well as other scenarios are explained in Boechat Albernaz et al. (2020).

RESULTS

This section describes the new results from the diatoms, updated mouth closure reconstructions, the crevasse and levée evolution and the numerical modelling. In the synthesis, these new pieces of information are combined and integrated with existing reconstructions to provide an updated overview of estuary evolution.

Diatoms show initiation of peat formation under brackish conditions

Landward diatom core (GW core)
The transition from tidal clays to reed peat (at 3.78 m depth) is most important for the reconstruction of tidal basin closure mechanisms. In the clays, the diatom assemblage is representative for marine–brackish conditions in an estuarine

Table 1. Salt to freshwater classification used in this study, after Van der Werff & Huls (1974).

Classification	Salinity
Marine	>17‰
Marine–brackish	5–17‰
Brackish	1–5‰
Brackish–fresh	0.1–1‰
Fresh	<0.1‰

environment. The first decimetre of reed peat on top of the clays contains diatoms that indicate brackish conditions during peat formation and terrestrialization in estuarine tidal environments (*ca* 27% increasing upward to >63% marine–brackish and brackish species combined, indicative of estuarine and tidal environments Fig. 3).

The unconsolidated clays (below 3.78 m depth) are dominated by coastal marine species (>50% – for example, *Campylosira cymbelliformis* and *Cymatosira belgica*) and marine–brackish species (for example, *Delphineis minutissima*, *Delphineis surirella*, *Planothidium delicatulum*, *Raphoneis amphiceros* and *Thalassiosira eccentrica*), importantly accompanied by estuarine species (for example, *Diploneis aestuari* and *Cyclotella striata*). The environmental conditions are typified by the autochthonous estuarine species, that indicate a brackish environment and the presence of a river mouth nearby (particularly *C. striata*; De Wolf, 1986a). Marine influence in the estuary is illustrated by the presence of marine–brackish benthic species. Here, littoral–pelagic species *C. cymbelliformis* (Van der Werff & Huls, 1974) that is only present in the clays and disappears in the peat, serves as the main indicator for marine influence, rather than the over-represented *C. belgica*. Marine–brackish (coastal) species are generally regarded as 'inwash' (allochthonous, similar to marine species) in non-marine environments and therefore treated as subordinate in the interpretation of palaeoenvironmental reconstructions (Vos & De Wolf, 1988). However, marine in and outflow is a fundamental characteristic of the estuarine environment and allochthonous marine–brackish species are therefore very useful as an indicator for the degree of marine influence in the tidal basin. The marine–brackish coastal species in this core are mainly tychoplanktonic, benthic and littoral–pelagic, which means that they live close to, on or in the substrate, respectively, and are not as easily

Table 2. Selected Delft 3D scenarios from Boechat Albernaz *et al.* (2020). These scenarios resemble key aspects in the evolution of overbanks of the Old Rhine since peat growth initiation (as reconstructed in this paper, see *Synthesis*).

| Number	Description	Old Rhine situation	Tides at mouth (m)	Fluvial discharge (m³ s)	Vegetation
96	High tides (mouth still open) and reed in floodbasin	*ca* 5500–4500 cal BP	1.25	700	Dense (reed marsh)
74	Low tide (mouth closing) and wood in floodbasin	*ca* 4500–3800 cal BP	0.25	700	Sparse (Alder carr)
104	Low tide, river discharge increasing and wood in floodbasin	*ca* 3800–2800 cal BP	0.25	1500	Sparse (Alder carr)
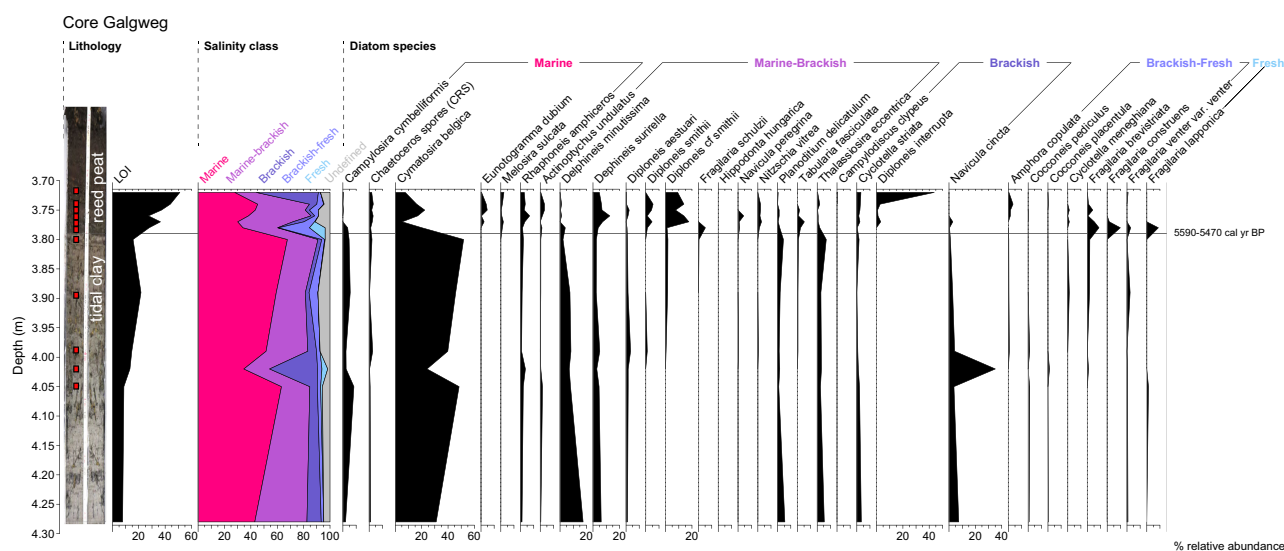
Fig. 3. Diatom analysis of the landward *GW* core (Galgweg). Left: data for environmental reconstruction including salinity conditions in colour (see Table 1 for salinity classes). Right: Diatom species with relative abundance >3% including *C. clypeus* and *N. vitrea*. Samples are indicated with green dots, samples at 3.66 m and 3.69 m are omitted for lack of countable valves. Date of base of peat after De Jong (1977). Locations are in Fig. 1, data can be found in Appendix S1, photograph selection in Appendix S2.

transported as planktonic species. Moreover, the share of attached valves (i.e. not substantially damaged) of marine tychoplanktonic species in the counts was substantial, suggesting that these diatoms were probably not transported over large distances or under highly energetic conditions. Therefore, the allochthonous marine–brackish species were probably not solely transported into the back-barrier basin by occasional storm surges, as may have been the case for marine (planktonic) species, but part of the estuarine environment with regular tidal influx. The conditions in the back-barrier basin were likely subtidal to inter-tidal, illustrated by the occurrence of *Navicula*

cincta and its peak in relative abundance at 4.02 m depth in the clay. *Navicula cincta* has a wide salinity tolerance (to brackish–fresh – Van der Werff & Huls, 1974; marine–brackish – Vos & De Wolf, 1993; Walker *et al.*, 1998; Hassan *et al.*, 2006) and can be associated with saltmarsh environments (Sawai *et al.*, 2018) or drier conditions (De Wolf, 1981). The peak should therefore be interpreted with care. Here, *N. cincta* occurs simultaneously with a slight peak of aerophilous *R. amphiceros*, an increase in organic matter content and flat *Phragmites* rhizome remains. Slightly drier conditions (temporary or occasional) on tidal flats are deemed the most likely
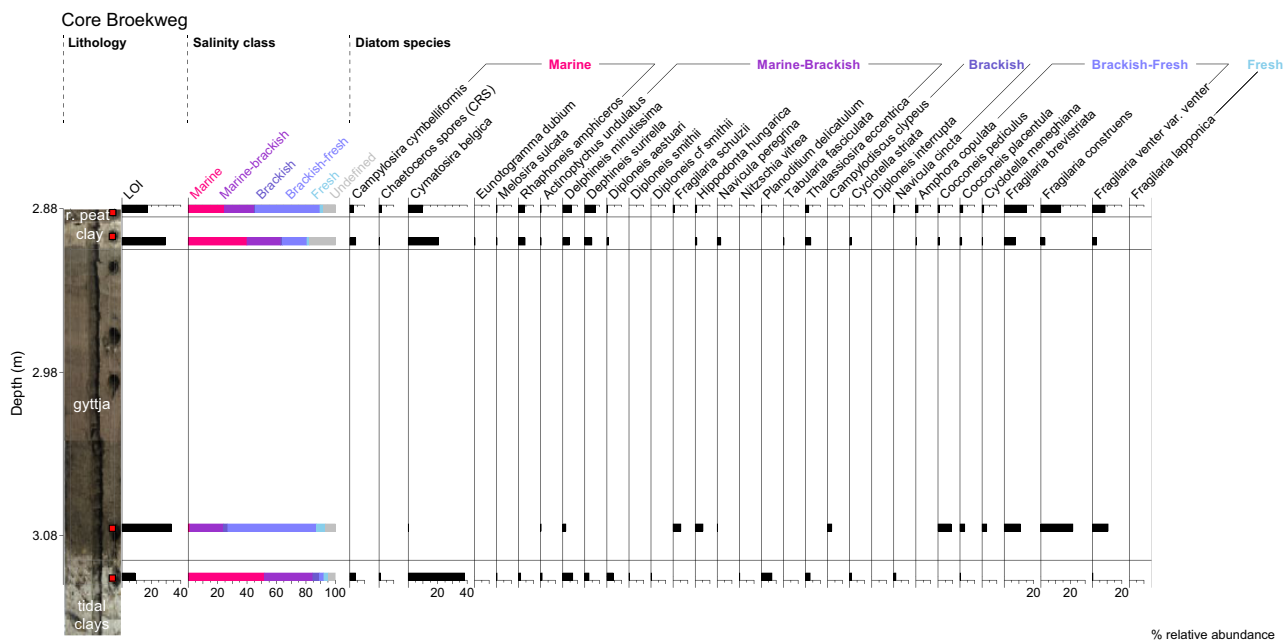
Fig. 4. Diatom analysis of the seaward *BW* core (Broekweg). Fewer samples were analyzed, because the *BW* core serves for support. To prevent distortion of the signal, the data is depicted as bar graphs. Left: data for environmental reconstruction including salinity conditions in colour (see Table 1 for salinity classes). Right: Diatom species with relative abundance >3% including *C. clypeus* and *N. vitrea*. Samples are indicated with green dots, for location (see Fig. 1). Data in Appendix S1, photograph selection in Appendix S2, see Fig. 5H for position of the core in cross-section.

interpretation. There are no signs of consolidation or soil formation in the clay, and characteristic species of the upper intertidal zone and salt marsh, that do appear in the *Phragmites* peat, are absent in the clays. Therefore, it is clear that terrestrialization did not progress at that time of clay deposition. The combined characteristics of the diatom assemblages in the clays (estuarine autochthonous species, marine–brackish benthic and littoral–pelagic species, occasional peak in aerophilous species of tidal flats) provides a clear signal that the Old Rhine embayment was an estuary where subtidal and intertidal conditions prevailed. A river was present, but fluvial (freshwater) influence was limited. The abundant exchange with marine waters shows that the estuary still stood in open connection with the sea.

At the onset of peat formation, the contact between the tidal clay and the reed peat is sharp (3.78 m depth, LOI increase from 20% to >30%). Directly above this transition, a clear terrestrialization trend is visible in the diatom assemblages of the lower centimetres of peat. The valve density in the peat decreased upward with signs of dissolution, no diatoms were encountered from 10 cm above the clay–peat contact. Dissolution of valves in peat is not uncommon because reed

consumes silica (De Wolf, 1986a,b). The onset of peat formation coincides with the prominent expansion of *Diploneis* (cf.) *smithii*, a marine–brackish species living in the substrate (Vos & De Wolf, 1993) and attributed to lower marshes and tidal flats (Sawai *et al.*, 2002). Other important autochthonous indicators are *Nitzschia vitrea*, that is linked to brackish environments where terrestrialization is in progress (De Wolf, 1981), *Nitzschia navicularis* that lives on higher parts of mudflats with sparse vegetation, and *Navicula peregrina* that occupies the highest (vegetated) parts of estuarine flats (De Wolf, 1986a,b). *Diploneis* sp and *Navicula digitoradiata* are also associated with (vegetated) intertidal environments (Vos & De Wolf, 1988, 1993; Sawai *et al.*, 2002). The anomalous peak in Fragilaria species (*F. construens, F. lapponica, F. nitzschioides, F. schulzii*, classified as brackish–fresh, fresh, brackish–fresh and marine–brackish, respectively) at the onset of peat formation could point to stagnating (light) brackish shallowing waters (De Wolf, 1986b; Denys, 1989), but are also indicative of a relative increase *of Phragmites* habitat as opposed to mud habitat (Marco-Barba *et al.*, 2019). The latter interpretation is more likely given its occurrence in *Phragmites* peat and

the presence of other diatom assemblages indicating brackish inter to supratidal conditions. In this case, the small peak of fresh diatoms in Fig. 3 at 3.78 m does therefore most likely not indicate fresh conditions nor a strong freshwater influence. A few centimetres upward (3.72 m depth), *D. interrupta* becomes abundant, indicating the development of a salt marsh with *Phragmites* vegetation (Vos & De Wolf, 1993). The relative abundance of coastal marine allochthonous species (*C. belgica* and *D. minutissima* etc.) strongly declines in the peat and, importantly, marine littoral–pelagic species *C. cymbelliformis* disappears. This points to a decrease of marine influence in the estuary, either because the open connections with the sea were closing (beach-barrier formation) or because the expanding reed fields allowed for marine inflow to penetrate less far into the back-barrier basin. In any case, the marine–brackish diatom assemblages in the peat clearly indicate a terrestrialization process of the tidal environment by peat formation under brackish conditions.

Seaward diatom core (BW core)

Seaward core *BW* was used to substantiate the detailed findings of the landward *GW* core, in particular for comparison of salinity and environmental conditions in the clays and peat. Core *BW* was sampled in lower resolution, but displays a generally comparable succession from tidal back-barrier clays to peat, but with some differences (Fig. 4). Contrary to the clay–peat transition of the landward core, *BW* first contains gyttja on top of the tidal back-barrier clays, with a thin clay layer on top. Reed peat is present on top of that clay layer, and interrupted by more thin clay layers.

Diatom assemblages at the top of the unconsolidated (tidal) clays below the gyttja (below 3.10 m depth) indicate estuarine conditions and characteristic exchange with marine waters, comparable to those in the landward core tidal clays, with *C. cymbelliformis* and *C. striata* as main indicator species (Van der Werff & Huls, 1974; De Wolf, 1986a). The lower gyttja (3.08 m depth) is dominated by brackish–fresh *Fragilaria* and *Cocconeis* species (*F. brevistriata, F. construens, F. venter* var. *venter, C. pediculus, C. placentula*), and several marine–brackish species, that particularly point to calm waters (*Campylodiscus clypeus, Hippodonta hungarica, Navicula salinarum* and *Fragilaria ulna*). Epiphytic diatoms (*C. pediculus* and *C. placentula*) suggest the presence of water plants (Van der Werff & Huls, 1974). Marine (coastal) diatoms

are virtually absent. This shows that the gyttja developed in an initially brackish quiet pond that was likely cut off from surrounding waters. The gyttja now appears to be located in a depression in the subsurface (see Fig. 5I). Given the presence of the overlying crevasse deposits that may have caused significant compaction, it is likely that this pond was slightly elevated in the surrounding landscape at the time, so that it was relatively isolated from the tidal basin.

In the clay layer on top of the gyttja (2.90 m depth), the diatom assemblages show a return of marine waters to this location (*C. belgica, C. cymbelliformis, Delphineis* sp., *R. amphiceros* and *T. eccentrica*). A few centimetres upward at the onset of peat formation, the diatom flora indicates brackish coastal flowing waters (*Delphineis* sp., *Fragilaria* sp., *N. cincta* and *Navicula distans*) with some water plants (*Cocconeis* sp.) and coastal marine influence or inwash (*C. belgica, C. cymbelliformis, R. amphiceros* and *T. eccentrica*). Characteristic autochthonous diatom species of intertidal environments and salt marshes are few (*N. digitoradiata, N. peregrina, D. aestuari, C. striata* and *N. vitrea*), and the absence of most *Diploneis* sp. compared to the landward site is striking. Although the specific local palaeoenvironment is more difficult to reconstruct using diatoms, the salinity conditions can nevertheless be inferred. The share of marine–brackish diatom species remains high and there are no distinct signs of freshwater conditions, which means that initial peat formation occurred under brackish conditions.

The diatom assemblages in the clays and peat of the seaward *BW* core confirm the interpretation of the findings at the landward *GW* site, in that the intertidal conditions and exchange with marine waters prevailed in the back-barrier basin palaeoenvironment and, importantly, that peat formed under brackish conditions. The gyttja of the *BW* core displays a local signal of a pond forming at that location, whereas the more continuous signal of the *GW* core clearly displays the terrestrialization process at the onset of peat formation, that can be taken as representative for a wider area in the back-barrier basin.

An updated reconstruction of the estuary mouth evolution

To assess the tidal influence on estuary evolution, the estuary mouth evolution (most downstream 15 km) was reconstructed in more detail by
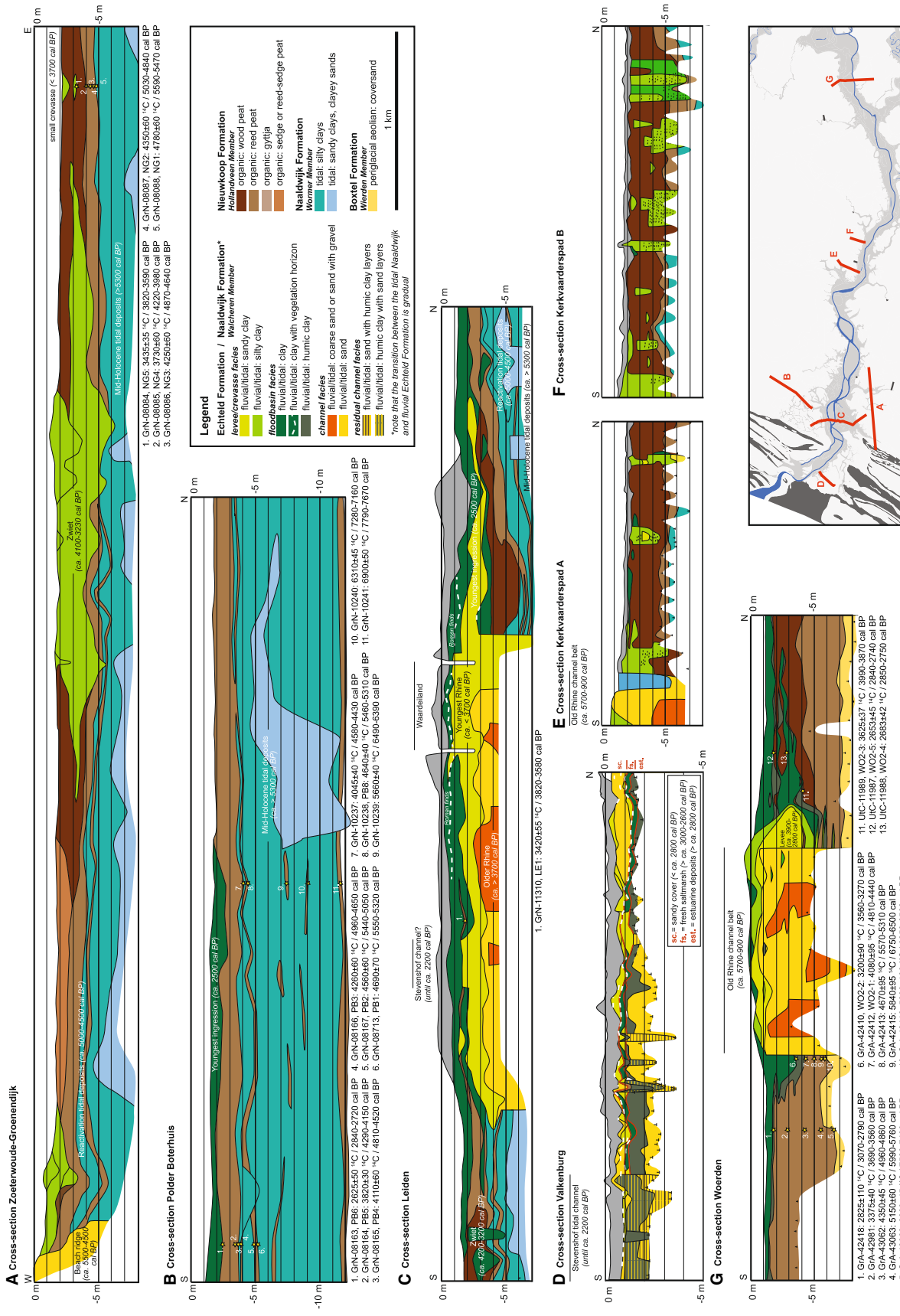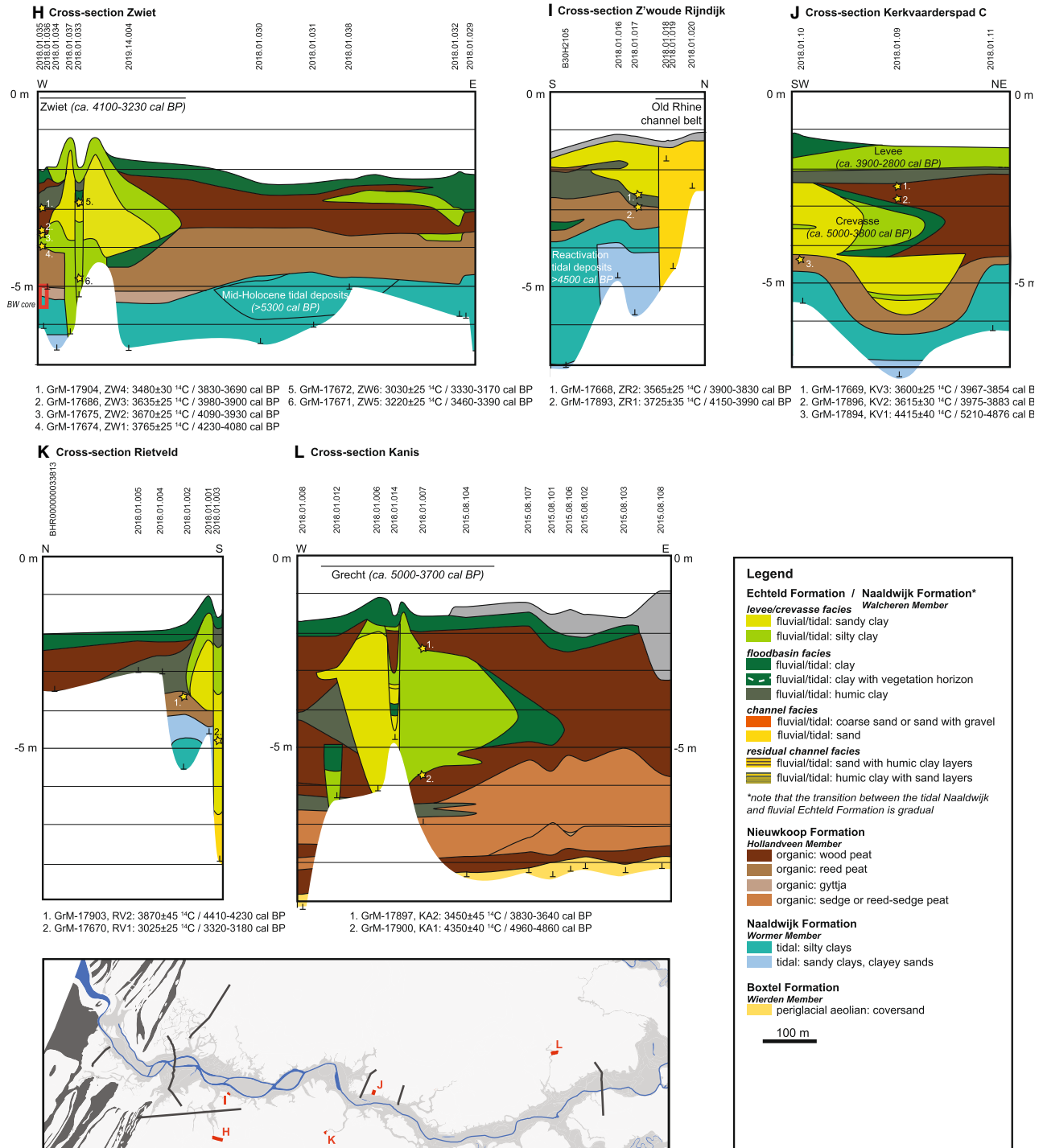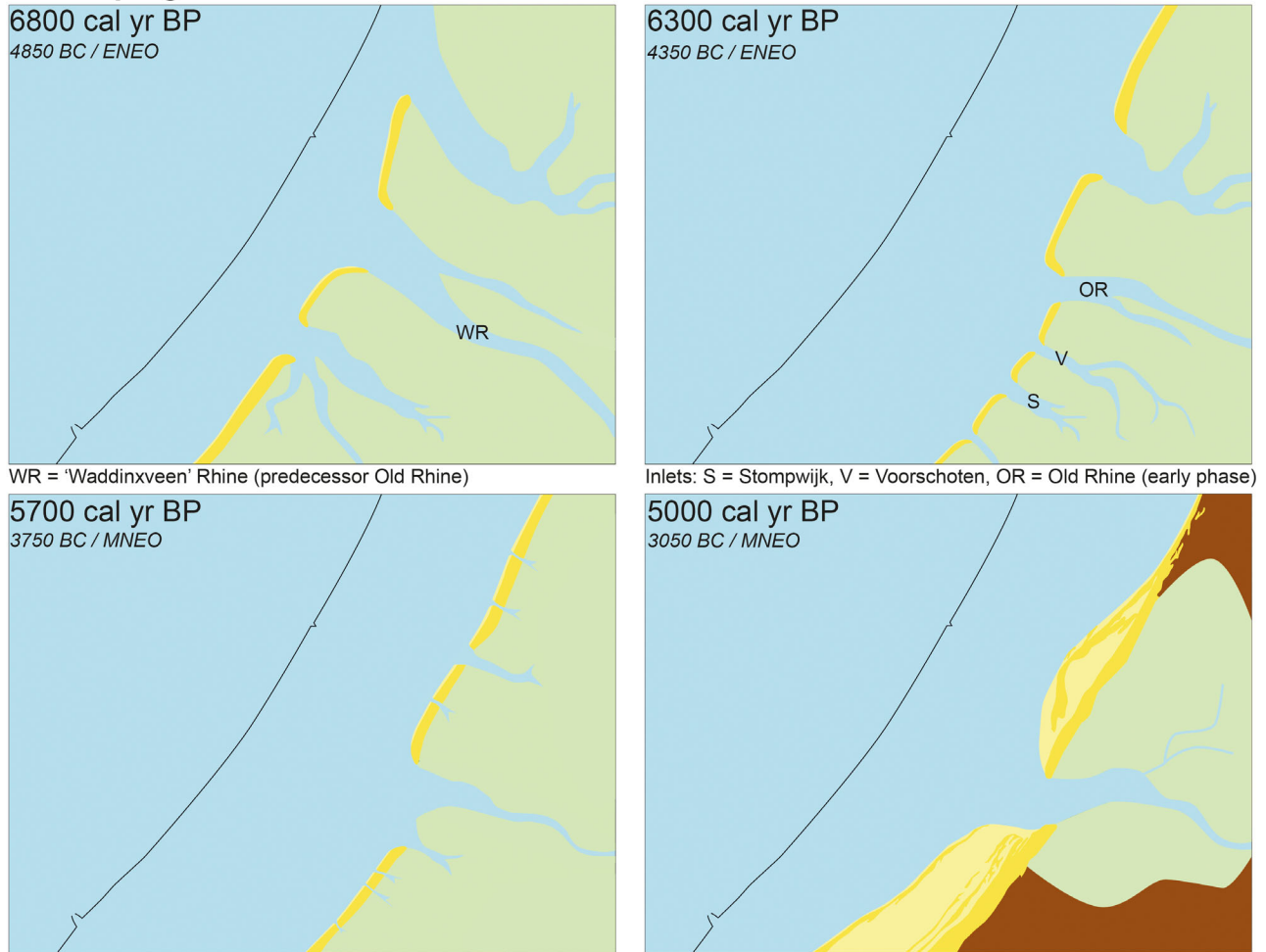
Fig. 5. (continued)

Fig. 5. Cross-sections in the study area, for location see Fig. 1. For the formation definitions in the legend see TNO-GSN (2022). *(part 1)* (A) Zoeterwoude-Groenedijk, after Van der Valk (1995). (D) Cross-section downstream: Valkenburg (after Tol & Jansen, 2012) note that vertical scale differs from other cross-sections. (B) Polder Boterhuis, after Van Der Valk (1995). (C) Leiden after Bosch & Pruissers (1979). (E) and (F) Kerkvaarderspad A and B after Kroes & Feiken (2011), (G) Woerden, after: Stouthamer (2001) and Van Asch (2007). *(part 2)* (H) Zwiet *(this study)*. (I) Zoeterwoude Rijndijk *(this study)*. (J) Kerkvaarderspad C *(this study)*. (K) Rietveld *(this study)* and (L) Kanis (*this study*, partly after van Asselen *et al.*, 2018).

© 2022 The Authors. *Sedimentology* published by John Wiley & Sons Ltd on behalf of International Association of Sedimentologists., *Sedimentology*

Barrier progradation and back-barrier sedimentation
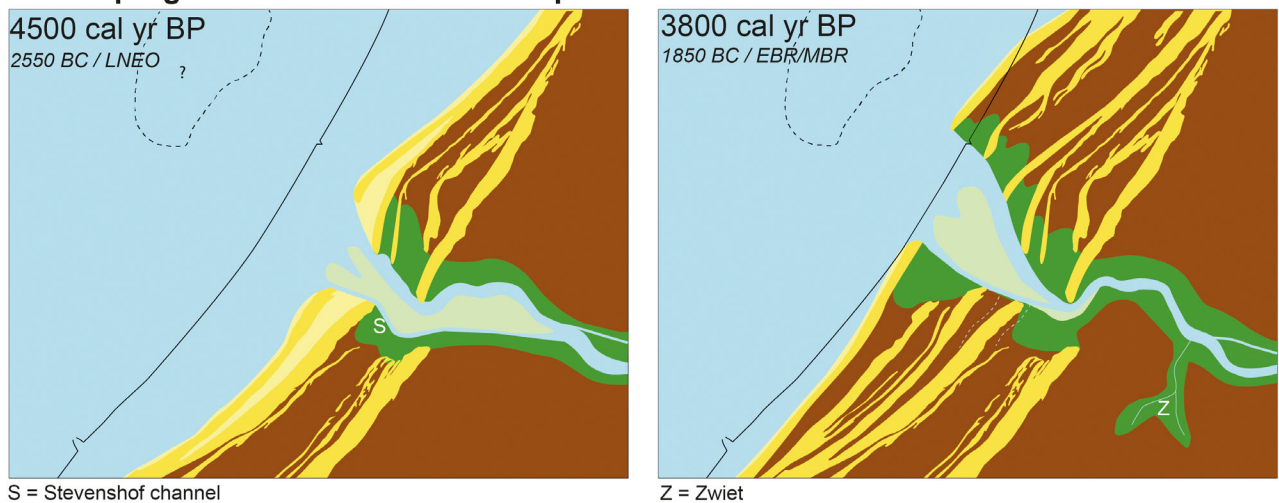

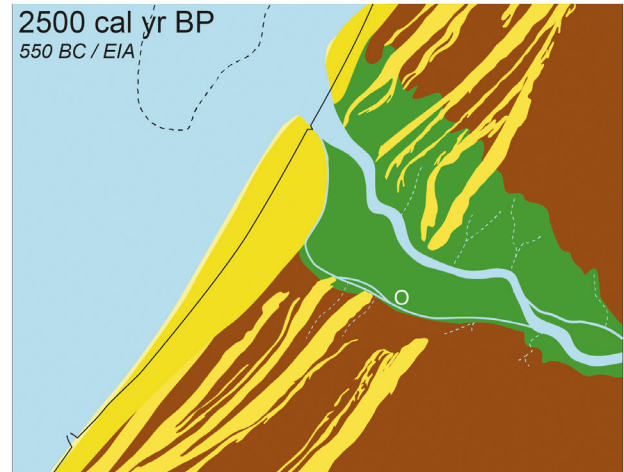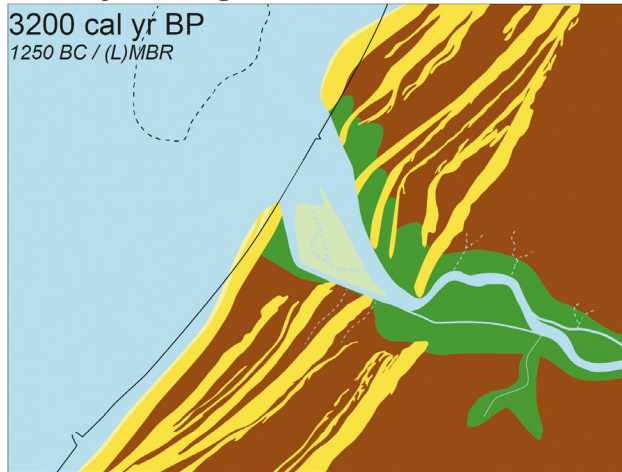## Barrier progradation and back-barrier peat formation
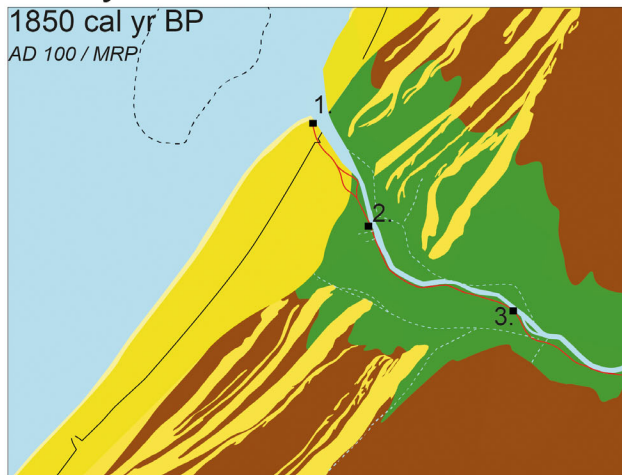

Fig. 6. Updated palaeogeographical reconstructions of the downstream *ca* 15 km of the Old Rhine estuary. Mouth closure and crevasse ages are updated relative to De Haas *et al.* (2019), based on data presented in this paper. The system gradually evolves from tidally-dominated basin into a peat-bounded tidal river and fills in in phases. For Dutch archaeological periods see Table 4.

Fig. 6. (continued)
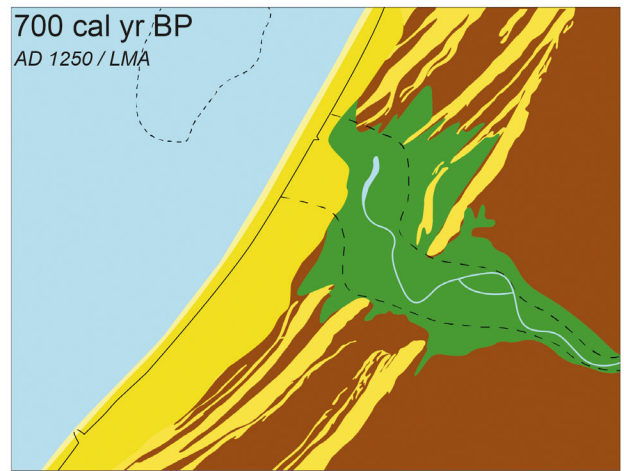
combining existing regional reconstructions of De Haas *et al.* (2019) with new local results from archaeological excavations. These latter studies locally mapped and dated the estuary substrate in high detail (notably Tol & Jansen, 2012; Meijer *et al.*, 2020), providing new key evidence for the position of the channels, bars and marshes over time.

Overall, a narrowing and infilling trend of the downstream 15 km of the estuary between *ca* 4000 and 2500 BP is seen. Until *ca* 2500 cal BP, two parallel main channels existed from the mouth up to km 20 upstream, with a relatively wide intertidal area in between, which accreted to a supratidal environment as the estuary filled in (Figs 5D and 6). The most downstream

Table 3.   Radiocarbon dates acquired in this study, see Fig. 1 for the locations and Fig. 5 for the position in the cross-sections. For legacy dates see De Haas *et al.* (2019, Supplements).

Code	Name*	Lab-id (GrM ....)	X/Y (m)†	Below surface (cm)	BP ± 1σ	Cal yr BP (1σ)‡	Material and stratigraphy	Reference
ZR1	Hazerswoude A-II-1	17893	97496/460891	189–191	3725 ± 35	4147–3989	Peat below fluvial levée	
ZR2	Hazerswoude A-II-4	17668	97496/460891	172–174	3565 ± 25	3898–3832	Peat below fluvial levée	
KV1	Kerkvaarderspad A-IX-1	17894	107648/459060	295–297	4415 ± 40	5210–4876	Peat below fluvial levée/crevasse	
KV3	Kerkvaarderspad B-I-1	17669	107733/459219	111-–	3600 ± 25	3967–3854	Peat below fluvial levée	
KV2	Kerkvaarderspad B-II-1-5	17896	107733/459219	124–130	3615 ± 30	3975–3883	Peat below fluvial levée	
KA1	Kanis A-II-1-2	17900	120864/459802	425–429/433?	4350 ± 40	4960–4860	Peat below crevasse levée	
KA2	Kanis A-I-1-3	17897	120864/459802	78–82	3450 ± 45	3830–3640	Peat on top of crevasse levée	
ME1	Meije A-I-1	17901	112137/458671	373–375	3540 ± 35	3890–3730	Peat below crevasse levée	
RV1	Rietveld C-II-1	17903	103860/457022	165–167	3870 ± 45	4410–4230	Peat below crevasse levée	
RV2	Rietveld A-I-1	17670	103888/456968	300–310	3025 ± 25	3320–3180	Detritus in crevasse residual channel	
ZW1	Zoeterwoude B-II-1	17674	95817/458051	201–203	3765 ± 25	4230–4080	Peat below oldest crevasse levée	
ZW2	Zoeterwoude B-III-1	17675	95817/458051	158–160	3670 ± 25	4090–3930	Peat on top of oldest crevasse levée	
ZW3	Zoeterwoude B-III-4	17686	95817/458051	146–148	3635 ± 25	3980–3900	Peat on top of oldest crevasse levée	
ZW4	Zoeterwoude B-I-1-3	17904	95817/458051	108–114	3480 ± 30	3830–3690	Peat below youngest crevasse levée	
ZW5	Zoeterwoude A-II-1	17 671	95881/458038	265–270	3220 ± 25	3460–3390	Detritus in crevasse residual channel	
ZW6	Zoeterwoude A-III-1	17672	95881/458038	128–131	3030 ± 25	3330–3170	Detritus in crevasse residual channel	
MP1	Munnikenpolder-1	–	97204/462803	130	2960 ± 44	3210–3060	Bottom of peat on estuarine deposits	Blom & Roessingh, 2007 ADC rap 802
MP2	Munnikenpolder-2	–	97204/462803	100	2922 ± 41	3150–2990	Top peat below crevasse	Blom & Roessingh, 2007 ADC rap 802
19	Hazerswoude-1	GU32474	99348/461683	74	3209 ± 42	3460–3380	Tree in parallel channel	ADC rap
20	Hazerswoude-2	GU32475	99309/461527	85	2397 ± 42	2490–2350	Seeds in residual channel	ADC rap
OM3	Ommedijk-3	M185	90030/462955	?	3090 ± 20	3360–3250	Clay on peat below levée	Meijer *et al.* (2020)
OM4	Ommedijk-4	M210	90157/462930	?	3000 ± 16	3220–3160	Clay on peat below levée	Meijer *et al.* (2020)

* Site name - A/B: location on the site - I–IX: stratigraphic interval level - 1–5: stratigraphical sublevel (cm). † X/Y, Dutch grid. ‡ OxCal 2020, rounded by 10 (Reimer *et al.*, 2020).

southern parallel channel (*Stevenshof*) left a *ca* 10 m thick sandy channel fill with clay and detritus layers (Meijer *et al.*, 2020). Its final closure was estimated to be around 2200 cal BP (*OM* in Fig. 9; fig. 5D – Meijer *et al.*, 2020), for its upstream counterpart closure was dated at *ca* 2400 cal BP (*HA* at km 15 in Fig. 1 and Table 3).

Between the two parallel channels, the oldest signs of estuary infilling can be observed in Leiden (10 km from the coast), where subtidal/intertidal deposits are covered by clays and peat dated at 3820 to 3580 cal BP (Fig. 5C). Roughly a millennium later, a similar transition from subtidal/intertidal to a supratidal environment took place in Valkenburg (km 5, Fig. 5D). The subtidal/intertidal deposits are sandy, while their upper metres consist of (humic and silty) clay. Locally, wood remains occur in the top of these clays (Van Heeringen & Van der Valk, 1989), indicating quiet and fresh conditions. The end phase was dated at 3300 cal BP by Lenselink (1988) and between 3250 and 2850 cal BP by Tol & Jansen (2012: table 5.1). On top of these deposits, clays with soil horizons and peaty intercalations occur, dissected by creek deposits with narrow levées (Fig. 5D). Shell remains and diatoms from the creek deposits indicate a quiet freshwater environment with modest tidal activity. The creek levées were inhabited during the Late Bronze Age and in the Early Iron Age (for ages of the Dutch archaeological periods see Table 4) and the end of channel activity is dated around 2700 cal BP (Fig. 9; Tol & Jansen, 2012). A similar succession from tidal flats to a supratidal environment has been found near the current coastline at Katwijk (*KW* in Fig. 1 – Van Heeringen & Van der Valk, 1989; Van Der Valk, 1995; Van der Leije & Hamburg, 2014) and *Munnikenpolder* (Table 3). In Valkenburg, coarser overbank phases were encountered on top of this succession, dated around 2100 cal BP and in the second century BP (Tol & Jansen, 2012). Diatoms in these deposits point towards a renewed increase of marine activity.

Levée dimensions and age

Natural levées along the Old Rhine vary in thickness from a metre thick on top of the channel belt to up to 4 m thick in the floodbasin where compaction of underlying peat layers allowed for more accumulation of sediment (Van Asselen, 2011). Along the reach of the river (from Utrecht to the coast), the levées generally do not expand further than a few hundred metres into the floodbasin. They predominantly consist of silty loam, silty clay loam and silty clay, with a lateral fining trend, but without a clear fining-upward sequence. It can be seen that the largest preserved levées occur after 3800 cal BP, independently dated at three places along the Rhine: (Figs 5G, 5I and 9, Table 3). Hardly any levées from earlier overbank phases could be identified. Most likely, these earlier levées were very narrow and mostly reworked as the channel meandering caused lateral migration of the Rhine channel (Stouthamer, 2001). Only modest traces of older levées can be found in cross-sections *Woerden* and *Leiden* in Fig. 5C and G. This suggests that formation of wide levées was modest before 3800 cal BP.

Crevasse dimensions and age

The crevasses mainly occur between Leiden (km 10) and Woerden (km 40). Their channel belt sediments often consist of laminated loam or fine sand with detritus and clay layers, while the levées mainly consist of loam, silty clay loam and silty clay (Fig. 2). Three types of crevasses are distinguished here based on their length and planform: short, long and dendritic crevasses (Fig. 1). First these three types are considered in more detail and then their ages and age trends along the Old Rhine channel belt are discussed.

The short crevasses are 10 to 100 m wide and a maximum of 2 km long. They typically have two or three sub-branches and penetrate into the floodbasin perpendicular to the channel belt. Their frequency and length reduces away from the estuary mouth in line with observations by Van Dinter (2013). Figure 7 shows this modestly scattered trend in more detail. The mean length of the longer crevasses and upper standard deviation clearly decrease in upstream direction (from 1000 m and 1400 m at km 15, respectively, to 1000 m and 700 m at km 35). The small crevasses even disappear upstream from the knickpoint in channel belt gradient around km 40 (Figs 7 and 8). These trends confirm that the crevasses were formed under the influence of tidal backwater, as already suggested by, for example, De Haas *et al.* (2019). A second type of crevasse is those longer than 2 km (called 'perimarine' crevasses – Berendsen, 1982). Examples are *Grecht*, *Meije* and several unnamed crevasses (see Fig. 1). They can be over 10 km long and interconnected with other creeks in the peatland (Van Dinter, 2013). Long crevasses occur at fairly regular intervals of 7 to 10 km along the channel belt, pointing

Table 4. Subdivisions of archaeological periods since the Neolithic period in The Netherlands used in this study (ABR, 1992). Ages are in BC/AD (AD 0/0 BC = 1950 cal BP).

Period	Subperiod	Code (in Figs 6 and 9)	Begin	End
Neolithic period (5300–2000 BC)	Early-Neolithic period	ENEO	5300 BC	4200 BC
	Middle-Neolithic period	MNEO	4200 BC	2850 BC
	Late-Neolithic period	LNEO	2850 BC	2000 BC
Bronze Age (2000–800 BC)	Early-Bronze Age	EBR	2000 BC	1800 BC
	Middle-Bronze Age	MBR	1800 BC	1100 BC
	Late-Bronze Age	LBR	1100 BC	800 BC
Iron Age (800–12 BC)	Early-Iron Age	EIA	800 BC	500 BC
	Middle-Iron Age	MIA	500 BC	250 BC
	Late-Iron Age	LIA	250 BC	12 BC
Roman period (12 BC–AD 450)	Early-Roman period	ERP	12 BC	AD 70
	Middle-Roman period	MRP	AD 70	AD 270
	Late-Roman period	LRP	AD 270	AD 450
Middle Ages (AD 450–1500)	Early Middle Ages	EMA	AD 450	AD 1050
	Late Middle Ages	LMA	AD 1050	AD 1500
Modern period (AD 1500–present)	–	MP	AD 1500	Today

towards a peatland drainage function. Up to km 30, the crevasses are oriented eastward (tidal flood direction), while upstream they are oriented more perpendicular relative to the channel belt (in the river flood direction) (Fig. 1). The third crevasse type has a dendric planform and is encountered directly behind the beach-barrier complex (10–15 km) (*Zwiet, PB* in Fig. 1).

Crevasse deposits are encountered at multiple stratigraphical levels, for example, cross-sections in Fig. 5E and 5F show at least three (undated) generations. Although most crevasses are visible in the current relief (due to past medieval peat compaction and oxidation in the surrounding floodbasins), some older ones are not clearly expressed in current topography and can therefore only be traced in cross-sections and borehole data. Our eight radiocarbon dated crevasses show levée sedimentation between 5000 and 3000 cal BP (Table 3; Fig. 9). So far, undated crevasses most likely date in the same age range, based on their stratigraphic position and context. Strikingly, crevasses seem to have mainly formed in the *Alnus* peat and to a lesser extent in the *Phragmites* peat. The oldest crevasse activity was encountered at site *SV* by Diependaele & Drenth (2010). Here, crevassing already initiated around 5300 cal BP, not long after peat formation in the floodbasin had started (Fig. 9). The crevasses bear Neolithic artefacts and show several reactivation phases until the Middle Iron Age (2450–2200 cal BP) (Diependaele & Drenth, 2010; p. 271), indicating that they

formed relatively high and dry landscape elements during these periods. For archaeological periods see Table 4. For the *Zwiet* and *Meije* crevasses, three and two sub-phases of overbank deposition were observed, respectively (Fig. 5H). No trend in sub-phasing along the 50 km longitudinal section was encountered (Fig. 9). Some younger crevasses (after 3000 cal BP) show reactivation (for example, *Meije*), with the exception of crevasses closer towards the coast (for example, dendritic *PB – ca* 2600 cal BP Fig. 9).

Crevasses have their highest top currently between 0.6 m and 1.1 m below current sea level, which is generally up to a metre above mean sea level at the end of crevasse activity (Fig. 9). Assuming some post-depositional loading and surface levelling this is an underestimation, which underlines that their levée formation took place during high water levels. The highest locations of the crevasse levées are consistently lower than the preserved levées on the Old Rhine channel belt, as a result of flood dampening into the vegetated floodbasin, their older age and compaction of underlying peat.

Crevasse and levée morphology in model scenarios

The model scenarios shed light on the morphological effects of tides, fluvial discharges and floodbasin vegetation that may have shaped the Old Rhine estuary.
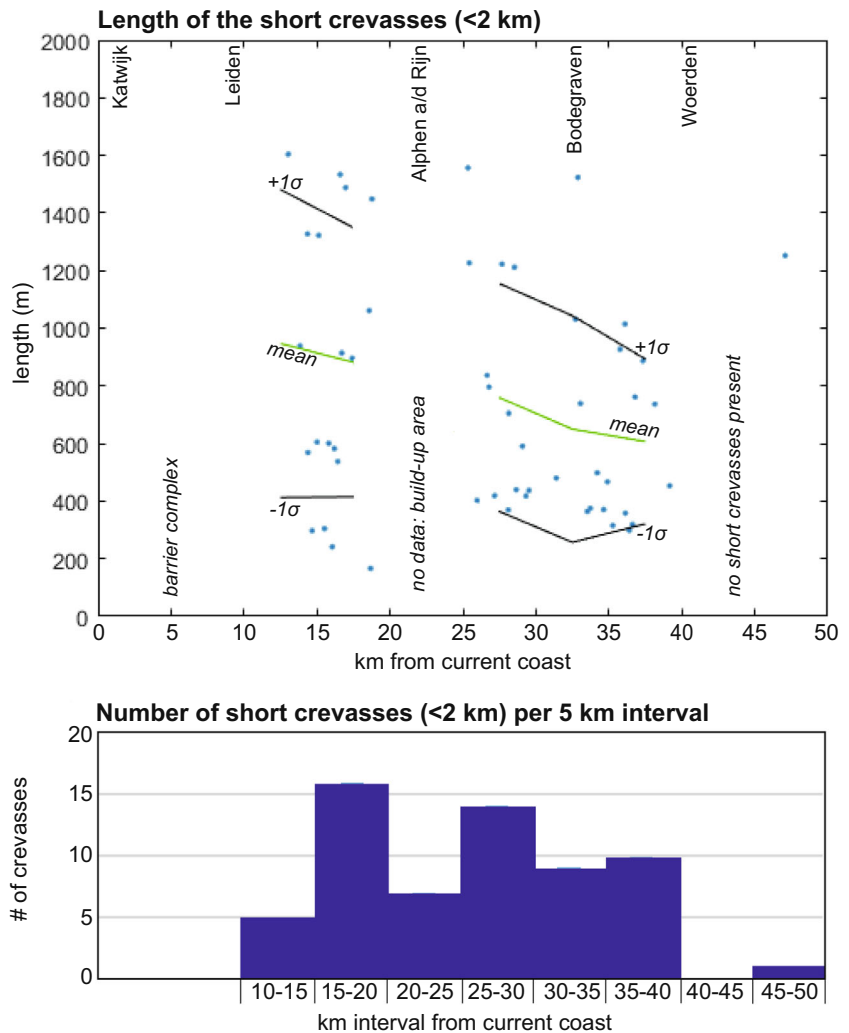
Fig. 7. Length of the short crevasses (<2 km) becomes progressively larger (B) and they become less frequent (C) towards the mouth. Length is measured using modern LiDAR images, assuming that peat compaction reveals most generations of crevasses as ridges.

In the first scenario (Fig. 10; model 96 – resembling the situation roughly 5500–4500 cal BP) it can be seen that, despite the high tidal range, no large crevasses form in a *Phragmites* filled floodbasin. These results confirm our field observations that floodbasin vegetation strongly controls levée and crevasse morphology; crevasses seem nearly absent in the stratigraphical record when large *Phragmites* marshes are present roughly before 4500 cal BP (Fig. 9). In the model scenarios with dense vegetation, crevasses are absent and relatively narrow levées are produced. This is because the dense vegetation in the floodbasin dampens the fluvial–tidal flow from channel to floodbasin and inhibit crevasse formation and avulsion (also observed in Nienhuis et al., 2018). It therefore decreases the bed shear stress and hence reduces the sediment transport from the channel towards the basin during high water. This phenomenon results in narrow levées and fewer crevasses (see also

Boechat Albernaz et al., 2020). Dense vegetation also causes mean water levels in the floodbasin to be higher in comparison to water levels in the channel. This combination of water level gradient and lower shear stresses further inhibits crevasse formation.

In the second scenario (Fig. 10; model 74 – roughly corresponding to 4500–3800 cal BP) lower tides and *Alnus* vegetation are seen in the floodbasin. The combined effect of tides and fluvial discharge with sparse (i.e. less dense) vegetation creates crevasses, despite the lower tidal range in comparison to scenario 1. This is because, in contrast to less dense vegetation, woods facilitate more crevasses and develop wider levées (Fig. 10). Sparse vegetation allows for more water flux from the channel towards the basin, which creates more shear stress and increases sediment transport. In addition, contrary to the dense vegetation scenarios, the water level gradient perpendicular to the channel
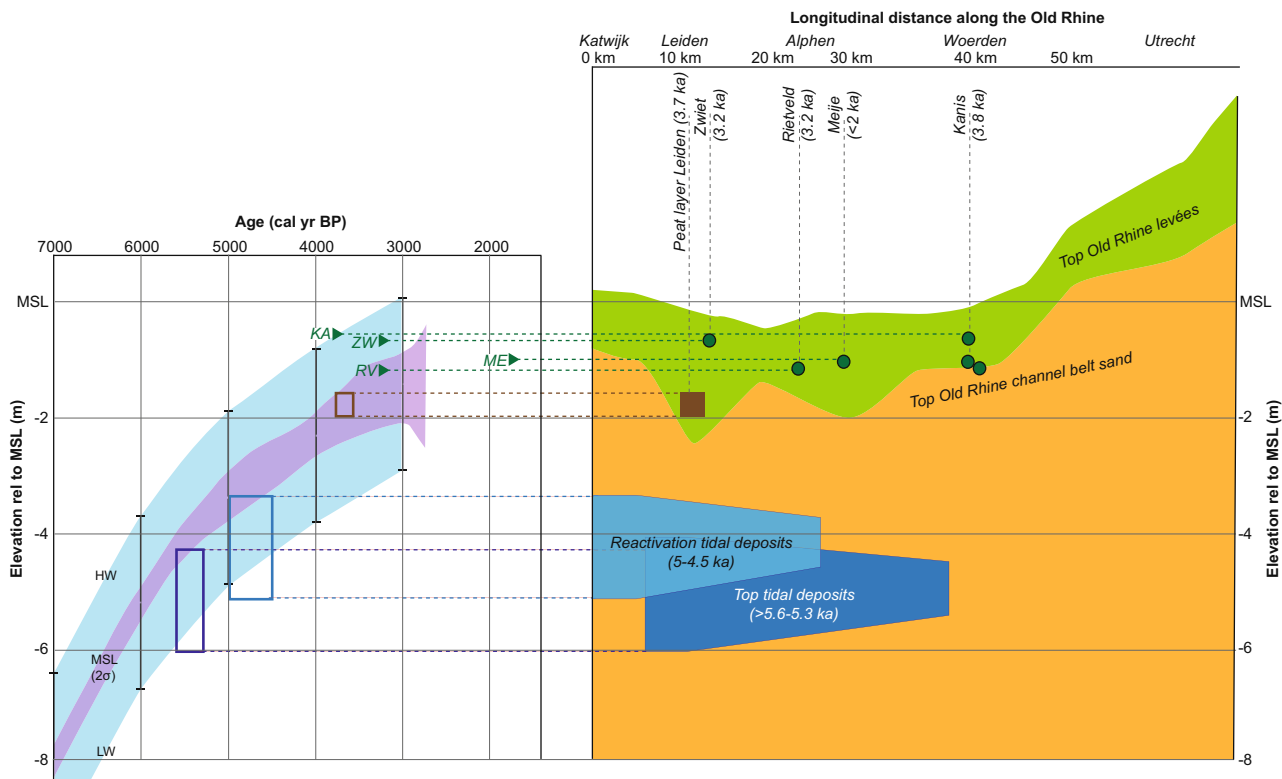
Fig. 8. Crevasse elevation, Old Rhine channel and levée slope in relation to Holocene sea-level rise (Hijma & Cohen, 2019). Tidal deposits older than 4500 cal BP, plot below sea level, confirming their intertidal facies interpretation. All crevasses plot above the SLR curve, indicating that they formed during high water events.

(from channel to floodbasin) is higher. These two factors combined allow for efficient formation and maintenance of crevasses under sparse vegetation conditions (Boechat Albernaz *et al.*, 2020).

The third scenario (model 104 – roughly 3800–2800 cal BP) is similar to scenario 2, but only includes higher river discharge, meaning that that the effect of tides became relatively smaller (e.g. Braat *et al.*, 2017). The model scenarios show that discharge fluctuations generated by tides induce more crevasses and allow levées to grow faster and larger. This is line with model scenarios by Boechat Albernaz *et al.* (2020) and confirms our field observations along the Old Rhine. Fewer crevasses are present after *ca* 3800 cal BP, because the mouth had silted up and fluvial discharge became higher. The effects of tides on crevasse formation are more pronounced in comparison with river floods because they promote daily water level variations while river floods are constrained to a few events per year.

SYNTHESIS: PHASES OF INFILLING

This section provides an updated synthesis with emphasis on new evidence on estuary infilling and associated mechanisms along the transition from tidal to fluvial dominated.

6000 to 4500 cal BP: from tidal basin to estuarine reed marsh

Until 5600 to 5300 cal BP (Fig. 9), an open tidal back-barrier environment existed in this part of the South Holland coastal plain. The Old Rhine branch captured one of its tidal inlets around *ca* 6000 cal BP (Hijma *et al.*, 2009; De Haas *et al.*, 2019). The top of the upper clayey part of the tidal deposits (Naaldwijk Formation, Wormer Member; TNO-GSN, 2022) is positioned between −4 m and −6 m below current sea level (Fig. 5A to C, E, F and H to K). This corresponds roughly to low water level at the coast at the time of formation (i.e. until around 5600 cal BP; Fig. 8). Diatom analysis of the top of the tidal
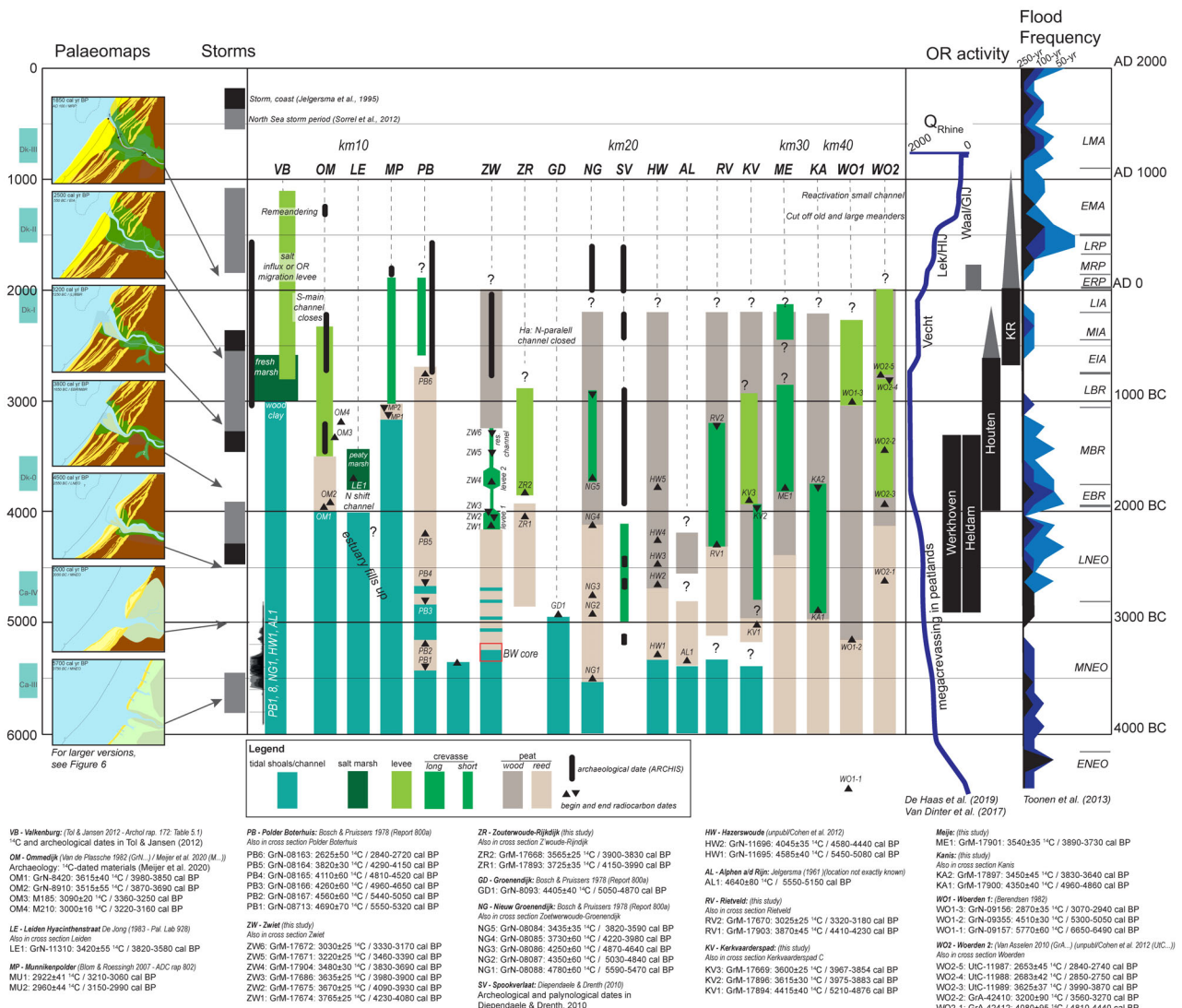
Fig. 9. Time–space diagram of overbank and floodbasin evolution along the Old Rhine (from *ca* 50 km upstream towards the coast) over the last 6000 years. Kilometre-positions and locations in Fig. 1. Calibrated radiocarbon dates (IntCal 2020) reported in 1 sig, rounded by 5. Most dates are also indicated in Table 3 and in cross-sections in Fig. 5. Dk/Ca = chronostratigraphical subdivision of The Netherlands (presumed transgression phases, in use until 2003) (Van der Valk, 1995). For Dutch archaeological periods see Table 4.

clays from two sites in the back-barrier tidal deposits indicates that marine–brackish shallow subtidal conditions prevailed, with occasional local shallowing or temporary drying of tidal flats. No freshwater influx indications have been found in sites *BW* and *GW*, suggesting that the Old Rhine River was not yet at full capacity. This confirms previous mollusc-based salinity reconstructions of 8 to 10‰ (marine–brackish cf. Van der Werff & Huls, 1974) by Raven & Kuijper (1981) for the upper metre of the tidal deposits (site *BH* in Fig. 1).

Reed vegetation was already modestly present in the tidal back-barrier area before peat accumulation started, as indicated by findings of horizontally oriented reed in the tidal clays. Large-scale *Phragmites* peat accumulation only started between 5600 and 5300 cal BP in a brackish tidal environment, rather synchronously (within a few centuries) along the river (Fig. 9; dates *PB1, NG1, HW1* and *AL1*). *Phragmites* indicates eutrophic conditions (Bos *et al.*, 2012), in the lowest centimetres the peat contains brackish diatom assemblages reflecting a terrestrialization
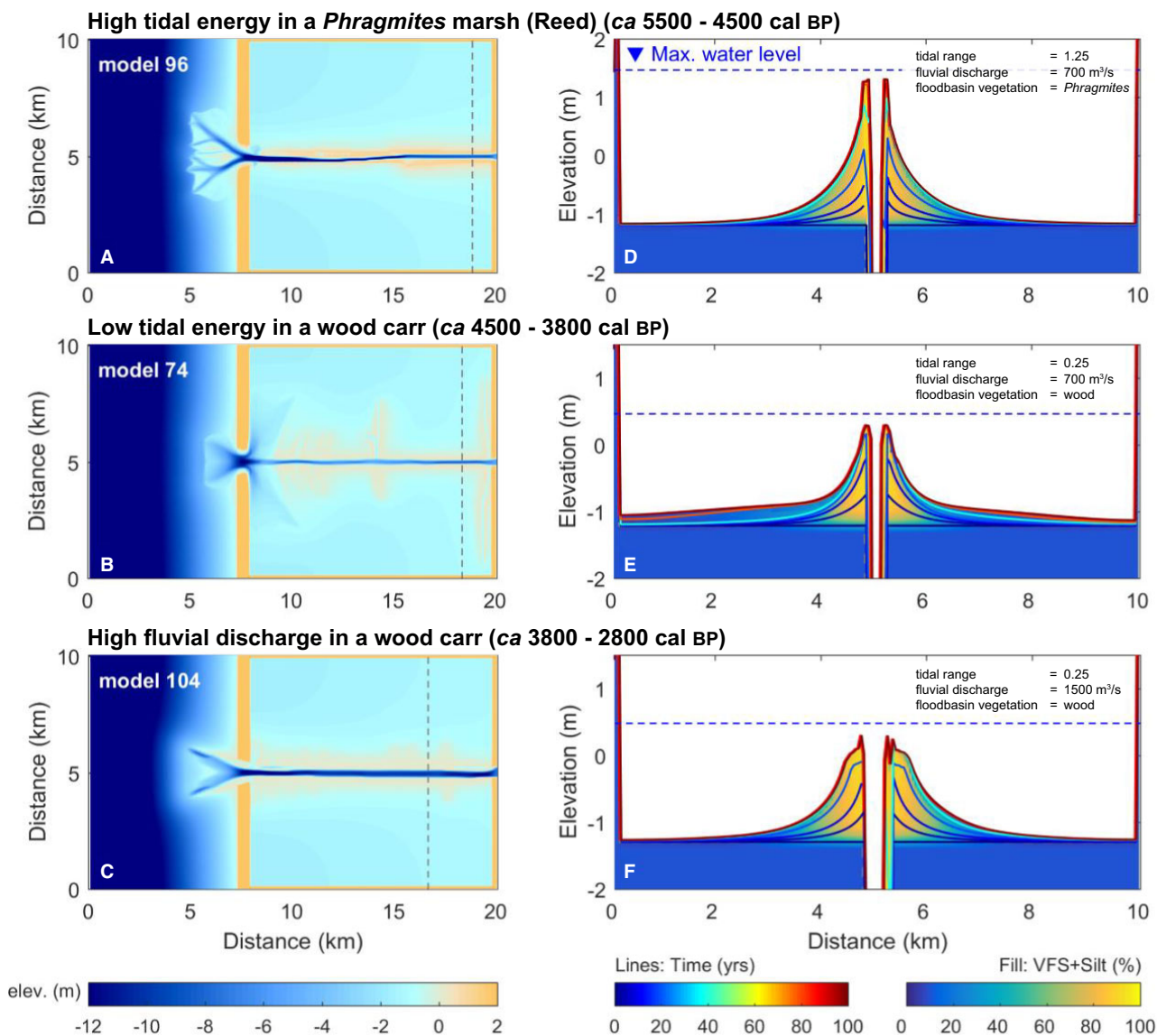
Fig. 10. Levées and crevasses after 100 years under a range of fluvial–tidal boundary conditions. Left panels (A) to (C) show the final plain-view morphology. Right panels (D) to (F) show the cross-section, illustrated in the correspondent map on the left, with combined percentages of very fine sand (VFS) and silt in the coloured fill scale and the bed level evolution shown in coloured lines.

sequence. In the reed marsh, ponds occurred locally, reflected by gyttja deposits and diatom assemblages of stagnant waters therein (site *BW*). Marine waters could still reach the back-barrier basin, as indicated by the marine–brackish (coastal) diatom assemblage in the peat and thin clay intercalations. No signs of a freshwater environment are found in the lower decimetres of reed peat. This indicates that beach barriers were probably still discontinuous or very low until *ca* 5300 cal BP. It implies that full barrier closure and subsequent back-barrier basin

freshening is not a prerequisite for initial peat accumulation, as is often hinted upon (Beets *et al.*, 1996, 2003; Beets & Van der Spek, 2000; Weerts *et al.*, 2005; De Wolf & Cleveringa, 2006; Vos, 2015; De Haas *et al.*, 2018). All peat encountered in the study area is part of the Nieuwkoop Formation, Hollandveen Member (TNO-GSN, 2022).

In the reed marshes along the Old Rhine, crevasses were rare (Fig. 9). No indications of early levées have been found that might have disconnected the estuary from the floodbasin

enhancing peat growth. Assuming lateral erosion by the river in younger stages, levées and their distal floodbasin clays have not reached more than a couple of hundred metres into the flood-basin.

After large-scale peat initiation, a local transgression occurred in the most downstream 20 km along the Old Rhine estuary (Fig. 9). In a zone of *ca* 5 km around Leiden, tidal deposits formed again until *ca* 4500 cal BP containing marine shells and covering the *Phragmites* peat (Bosch & Pruissers, 1979) (Fig. 5A to C and I). The clay layers and oxidation horizons 50 cm above the bottom of the peat in site *BW* are the distal edges of this, indicating flooding and fire events. Occasional marine influx reached at least until 20 km upstream around 4550 cal BP (Diependaele & Drenth, 2010; site *SV*), as indicated by diatoms, fish and vegetation remnants. This represents a final transgression phase into maturing reed marshes before peat formation fully took over.

4500 to 2800 cal BP: creeks and crevasses in the wood carr

After 4500 cal BP, accretion of beach barriers continued (Fig. 6), causing the coastline to approach its current position around 3700 cal BP (De Haas *et al.*, 2019). In the beginning of this period, the estuary mouth was still several kilometres wide. Its planform in the downstream 20 km was close to an 'ideal' trumpet-shaped estuary (cf. Savenije, 2015), with two large parallel channels with banks in between.

In the estuary floodbasins, peat growth continued. Floodbasin vegetation however, changed from *Phragmites* dominated to *Alnus* dominated (Fig. 5A, C, E to H and J to L). These *Alnus* wood carrs also hosted *Salix, Populus, Fraxinus, Ulmus* and *Corylus* (Havinga & Van Berg van Saparoea, 1982). This transition occurred diachronously along the Old Rhine between 5000 and 4000 cal BP (Fig. 9). Because *Alnus glutinosa* has a lower tolerance for water level fluctuation and brackish conditions (Den Held *et al.*, 1992), this transition indicates a shift towards fresh floodbasins with reduced water level fluctuation. Locally, oligotrophic bogs may have evolved (Kooistra *et al.*, 2013; Van Dinter, 2013), as indicated by blown-in *Sphagnum* remnants in the wood peat (Havinga & Van Berg van Saparoea, 1982). In the most seaward part, *Carex* (sedge) peat indicates slightly brackish

conditions directly behind the beach barriers (Van Dinter, 2013; Fig. 5A).

The new dates show that most crevasse sedimentation along the Old Rhine started between 5000 and 3800 cal BP (Figs 5H, J to L and 9). Most crevasse activity only started as the *Phragmites* marsh was replaced by *Alnus* carr (Figs 9 and 10; model 74). No indications have been found that their pathways were inherited from channels in the older mid-Holocene deposits. They seem to have newly formed as the floodbasins started to host wood carrs between 5000 and 4000 cal BP.

The long crevasses (>10 km long) most likely had a drainage function of the peat swamps as suggested by their lengths and regular spacing between them. At the same time, backwater-driven imported fluvial sediments could accumulate in their channels and on their levées. Their channels potentially formed a water route network for prehistoric inhabitants through the otherwise inaccessible peat areas of the Lower Rhine-Meuse delta (Van Dinter, 2013). Although sedimentation on many crevasse levées diminished from Late Bronze Age (*ca* 3000 cal BP) onwards (Fig. 9), their channels may have remained open longer, potentially keeping the water route network intact. For the *Rietveld (RV)* and *Zwiet (ZW/BW)*, dates on leaf detritus in their residual channel shows channel inactivity after *ca* 3200 cal BP (i.e. closure before Late Bronze Age Fig. 9).

Around *ca* 3800 cal BP, the dominant mode of overbank deposition changed from crevassing (with probably narrow levées that are not well-preserved) to wider natural levée formation along the entire channel belt (Figs 5G, I, J and 10; model 104). These trends correlate to further narrowing of the estuary in the lower 15 km, which has now been reconstructed in more detail (shoals become saltmarshes and become overgrown by peat at Leiden around 3700 cal BP – Fig. 5C). This probably reduced the effects of tides needed to create the crevasses. It also coincides with a possible increase in Old Rhine discharge to supply more sediments for the levées (resulting from upstream avulsion). Between 3200 and 2800 cal BP the tidal influence decreased further. From then onwards, estuary fills in with fresh (wood bearing) clays at site *VB* (Fig. 9) and three crevasses close (Zwiet, Rietveld, Fig. 5H and K).

After 2800: loss of tidal and fluvial activity

In the downstream 20 km of the estuary, infilling continued with freshwater clay deposits in

Valkenburg (*VB*; Fig. 5D) and closure of large parallel channels occurred between 2500 and 2200 cal BP (sites *OM* and *HA* Figs 1 and 9). Wave-driven alongshore sediment from the south formed a spit near Katwijk that nearly closed off the estuary (Fig. 6). This most likely happened as part of the overall infilling trend, but was probably aided by river discharge decrease, as the Utrechtse Vecht routed away *ca* 10% discharge from 2800 cal BP onwards (Bos *et al.*, 2009; Van Dinter *et al.*, 2017; De Haas *et al.*, 2019; Fig. 9). All of these developments most likely further reduced the effects of tides further upstream along the Old Rhine.

Decreasing fluvial and tidal sediment supply likely caused a decrease in levée and crevasse sedimentation (Fig. 9). After their sedimentation had stopped, many levées and crevasses in the peatland (with their tops around 1 m below current sea level, Fig. 8) became at least partly covered by peat as groundwater levels rose further. Its upper parts have disappeared again since Medieval reclamation (Borger, 1992), resulting in oxidation and compaction of the upper peat beds.

Although the overall effects of tides may have reduced gradually since *ca* 3800 cal BP, the effects of storm surges were probably larger as fluvial discharge decreased after 2800 cal BP (cf. De Haas *et al.*, 2019). This may explain the coarse-grained overbank deposits with marine diatoms covering the VB site between *ca* 2200 to 800 cal BP (Tol & Jansen, 2012; Fig. 5D). Also, new dendritic creeks evolved likely after 2800 cal BP (assuming some peat oxidation at the top of the peat) just behind the beach barriers (*MP* and *PB* in Fig. 9), covering peatlands with clay (Fig. 5B and C; Bosch & Pruissers, 1979). Clay was also deposited in between the northern beach barriers (Van der Valk, 1995; Fig. 6). These tidal reactivation clastic deposits are part of the Naaldwijk Formation, Walcheren Member (TNO-GSN, 2022). Its formation can likely be linked to coastline regression around the mouth and decreasing fluvial discharge (Figs 6 and 9).

The position of forts along the Roman *limes* corresponds to the localities where long crevasse channels connect to the Old Rhine (Van Dinter, 2013, fig. 4). Our results confirm that the Meije channel was indeed open during Roman Age (Zwammerdam). Also near site GD (Fig. 1) two minor crevasse channels remained open in Roman times (De Bruin *et al.*, 2022), but for the other creeks the presence of an open channel during Roman Age could not be confirmed. Habitation of the crevasse levées was possible, but given their vertical position and lack of artefacts, a decent portion of them was likely overgrown by peat in Roman times.

After Roman Age, upstream avulsion caused to Old Rhine discharge to become so low that its channel became much narrower. Around AD 800, a reactivation occurred near Utrecht (km 40–50), with smaller meander wavelengths and small flanking levées formed on top of the old channel belt (Van Dinter *et al.*, 2017). Also near the coast (km 0–15), a meandering reactivation likely took place between AD 400 and 1000. The already reducing fluvial activity essentially stopped when the river was dammed in AD 1122, upstream near Wijk bij Duurstede. This transformed the Old Rhine into a river with a regional to local drainage function. At the end of the 12th century, a dam was erected around km 30 (Zwammerdam Hendrikx, 1983; Van de Ven, 1993), to prevent water flow from upstream that likely could not drain fast enough due to progressive estuary closure. Tidal sedimentation in the downstream *ca* 10 km likely continued until the 12th century AD (demonstrated by estuarine shells dates in life position just behind the beach barrier – Van der Valk, 1995, and associated archaeological dates – Van Heeringen & Van der Valk, 1989). Final closure of the sea entrance took place as the progressive reduction of the fluvial discharge and tidal prism enabled coastal long-shore sand transport and dune formation to finally close the outlet (Van der Valk, 1995; De Haas *et al.*, 2019). The remaining Old Rhine channel and some of the open crevasse channels formed important natural waterways during and after the Medieval reclamation of these vast peatlands (Van Lanen & Kosian, 2020; Abrahamse *et al.*, 2021). Many of these old waterways still function in the current landscape, and their channel belts and levées appear as ridges in the landscape.

DISCUSSION

Vegetation and peat as landscape builders

Role in final phase of tidal basin infilling
The important role of vegetation in reducing tidal prism from the basins' edges has been highlighted by, for example, Vos & Van Kesteren (2000), De Haas *et al.* (2018) and Kleinhans *et al.* (2022) for the Dutch Holocene tidal

systems. This case study reveals that reed growth under brackish conditions can be effective during the final phase of infilling of tidal basins. After sediments fill the basin up to shallow subtidal levels, reed growth may start and accelerate the transition from brackish shallow conditions to full terrestrial conditions (*Basin infilling feedback* in Fig. 11). Reed marshes can become omnipresent, starting from the edges of the basin, as soon as back-barrier salinity and water depth become suitable for reed growth. Reed is known to tolerate brackish conditions via feedback mechanisms that reduce its salt stress (Reijers *et al.*, 2019). While its growth optimum is around 5‰, it can tolerate up to 15‰ salinity (Lissner & Schierup, 1997). Typical water depths of reed growth range from 0.2 to 0.5 m (Den Held *et al.*, 1992), the maximum water tolerated depth is between 0.6 m and 1.7 m (Weisner, 1987, 1991; Coops *et al.*, 1994). In tidal areas, lateral expansion by shoots or rhizomes is an effective form of reproduction of *Phragmites*, because the fluctuating water levels wash away seeds (Weeda *et al.*, 1991). Expansion of reed fields by rhizomes can occur at rates of *ca* 10 to 25 m/yr.

As reed starts to grow from the basin edges, a feedback mechanism sets in (Fig. 11). Reed slows down water flow at the edges of the tidal basin, which means that tidal range and prism of the entire basin are reduced (Boechat Albernaz *et al.*, 2020). Additionally, rhizomes and leaves accumulate as peat, taking up accommodation, further reducing the tidal prism. These two effects decrease tidal flow and enhance clay sedimentation throughout the remaining open part of the basin, leading to reduction of the tidal inlet cross-section (Jarrett, 1976). This means a further reduction in salinity and water level fluctuations. Under these circumstances, reed growth rates further increase (Deegan *et al.*, 2007; Engloner, 2009). Because of this positive feedback, reed growth can fill up brackish tidal basins effectively, in the Old Rhine case within a range of about three centuries (Fig. 9). This feedback shows that reed growth is not only a consequence of basin infilling but can also be an important cause behind it. While initial basin infilling may be controlled by waves, tides and sediment supply, a final infill and tidal inlet closure can likely be strongly controlled by vegetation.

A succession of back-barrier tidal sediments to reed peat certainly does not always indicate a transition from a salt/brackish to a freshwater environment, which is often implicitly assumed in (Dutch) lithostratigraphy (e.g. Weerts *et al.*, 2005). As is the case in our study area, reed peat is abundantly present in and in proximity to (brackish) tidal deposits along many coastal plains and estuaries, (e.g. Godwin, 1943 – UK; Pons, 1992 – NL). A brackish transition comparable to the *GW* and *BW* cores has been described for the Ilperveld in the North Holland coastal plain (some 40 km North of the Old Rhine, *ca* 20 km from the coast) by Bakker & Van Smeerdijk (1982). Here, brackish eutrophic reed peat initiation on top of tidal clays was dated around the same age (5465–5300 cal BP). Additionally, intercalations of peat (mostly reed) in tidal deposits are abundant along many other coastal plains and Holocene estuary infills in North-west European coasts (Pons & Wiggers, 1959/1960 – North Holland; Roeleveld, 1974 – northern Netherlands; Allen, 1990, 2000; Pons, 1992; Baeteman, 1999; Long *et al.*, 2000; Behre, 2007; Hijma *et al.*, 2009 – western Netherlands; Deforce, 2011 – Belgian coastal plain; Wartenberg *et al.*, 2013 – German Bight; Brew *et al.*, 2015; Hamilton *et al.*, 2019 – UK estuaries). Such intercalating coastal peat layers are often labelled as regressive surfaces, implying that they are caused by sea-level deceleration (or even drop) or morphodynamics. Our results, however, show that these may not (only) be the result of decreasing marine influence (Behre, 2007; Vos, 2015). Instead, vegetation growth and peat accumulation can also be a driving force behind these regression phases; vegetation hampers waterflow at the basin edges and subsequent accumulation fills up the basin.

The transition from *Phragmites* marshes to *Alnus* and *Salix* dominated wood carrs found along the Old Rhine between 5000 to 4000 cal BP, is common in the downstream parts of the Rhine-Meuse delta (Pons, 1992). In UK estuaries these transitions are commonly found as well (Waller & Kirby, 2021: Sussex Ouse valley – Waller & Hamilton, 2000; Waller & Early, 2015, in the western valleys of Romney Marsh – Waller, 1994, and the Thames estuary Devoy, 1979; Branch *et al.*, 2012; Waller & Grant, 2012). This succession is typical for shallowing water (Vermeer-Louman, 1934), but also reflects a decrease of saline water influx, lower water level fluctuations (−0.1 to 0.1 m), while nutrient input remains relatively high (Den Held *et al.*, 1992; Bos *et al.*, 2012 – Fig. 11; Table 5). These environmental changes gradually took place as floodbasins became more isolated from
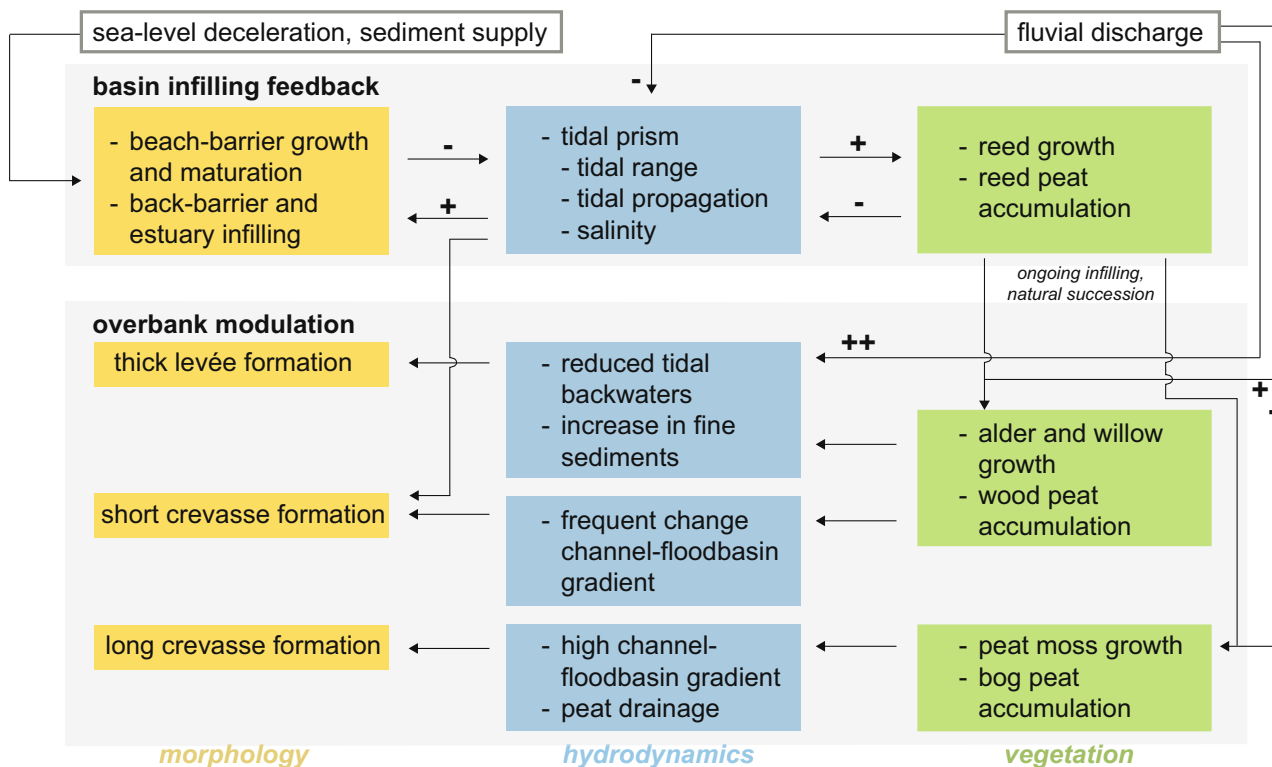
Fig. 11. Conceptual diagram of relations between morphodynamics, hydrodynamics and vegetation found in this study. *The basin infilling feedback* shows more sediment import in the back-barrier reduced tidal prism and salinity, allowing more sediments to be imported. This is strongly accelerated when a depth and salinity threshold for reed growth is reached. From that point onwards reed laterally grew into the basin reducing tidal prism and flow dynamics even further allowing for a faster infilling. As the peat swamp has established the *overbank modulation feedback* starts. Nutrient rich waters allow for alder growth (locally with bogs) that facilitates crevasse formation. An even larger fluvial input pushed out the tides and may allow for levée formation instead of large scale crevasse formation.

tidal influence when the estuary mouth of the Old Rhine became smaller and larger levées formed along the river. Fed by nutrients from the river, *Alnus* and *Salix* are typical for distal floodbasins in fluvial environments. Both the *Phragmites* marshes and the wood carrs still received a decent portion of clay during floods (Bos *et al.*, 2012). Where large rivers were absent in the Dutch coastal plain, a typical succession from eutrophic reed via mesotrophic sedge to oligotrophic *Sphagnum* peat is generally encountered instead (for example, south-west Netherlands Bennema & van der Meer, 1952; Pons & Wiggers, 1959/1960; Ilperveld – Bakker & Van Smeerdijk, 1982; Pons, 1992).

Shaping overbank morphology
In line with Nienhuis *et al.* (2018) and Boechat Albernaz *et al.* (2020) our case study shows that creek/crevasse morphology around estuaries is

not only steered by morphodynamics in the parent channel, but is also strongly controlled by the floodbasin vegetation and peat substrate (Fig. 11). Both field and model observations along the Old Rhine demonstrate that crevasses preferentially occur in wood vegetation and form less easily in denser reed vegetation. Because nutrient-rich river water facilitates wood carr growth with relatively low stem densities, this means that rivers can create their own crevasse-facilitating environment.

Higher flow resistance in denser reeds decreases shear stress and therefore inhibits sediment transport towards the floodbasin (Boechat Albernaz *et al.*, 2020). In reed marshes, however, water and fine sediments could still be locally dispersed though open spaces. Because wood carrs develop under nutrient-rich river water input, crevasses can form more easily because the stem density of the vegetation here

is lower. This means that small crevasses, while primarily driven by tidal backwaters, are facilitated by nutrient-rich river water supply that cause wood carr development in the floodbasins (Fig. 11). The longer crevasse systems (>10 km) additionally functioned as peatland drainage creeks. During storm surges and river peak discharge, they would temporarily experience significant water and sediment import (see *next section*).

The crevasses along the Old Rhine are all relatively elongated compared to reference cases that show much wider and shorter splays [for example, Columbia and Saskatchewan River, Canada – Smith *et al.* (1998), Makaske *et al.* (2002), Smith & Pérez-Arlucea (2004), Millard *et al.* (2017), or semi-arid (sandy) environments – Sandover River Australia; Tooth (1999, 2005), Millard *et al.* (2017)]. Comparable elongated crevasses are typically observed in peatlands as avulsion belt crevasses in the Rhine-Meuse delta (Makaske *et al.*, 2007; Pierik *et al.*, 2018); but also in tidal swamp landscapes, elongated creeks have been found connecting former channels and former peat domes, for example in the South-western Netherlands (*Schouwen Duiveland*; Kuipers, 1960; Pons, 1992); around the Oer-IJ (Pons, 1992; Vos *et al.*, 2015), and Ems estuary on the Dutch–German border (Behre, 2004). These crevasses reflect complex hydrological and nutrient regimes in often river-fed coastal swamps. They are not only comparable in morphology, facies and environmental setting, but most likely also in their hybrid nature of peat drainage and tidal crevasse functioning.

Importance of marine and fluvial boundary conditions

Role of sea-level rise
Holocene sea-level rise is one of the most important long-term boundary conditions for Holocene estuary evolution (e.g. Stanley & Warne, 1994; Hijma & Cohen, 2011, 2019; Smith *et al.*, 2011; Wang *et al.*, 2018). It first facilitates creation of accommodation and, as it decelerates, beach barriers and tidal back-barriers can be formed (Davis Jr & Clifton, 1987; Beets & van der Spek, 2000; Cattaneo & Steel, 2003; Cooper *et al.*, 2012; Fruergaard *et al.*, 2014 – Fig. 11). When it comes to a deceleration in sea-level rise, however, other factors seem to become more important. For the Holland coast, rates of sea-level rise have decelerated over the Holocene, but between 5000 and 3000 cal BP sea-level rise was nearly linear at *ca* 1 mm/yr (Hijma & Cohen, 2019; Fig. 9). This makes accelerated rates of sea-level rise an unlikely cause for more frequent crevasse initiation between 5000 and 3800 cal BP. The succession from reed to wood peat (affecting crevassing frequency) also seems to have occurred independently from changing sea-level rates. This is confirmed by the fact that older wood peat accumulation in the lower Rhine-Meuse delta (around 6500–7000 cal BP – Van der Woude, 1984; Hijma *et al.*, 2009) took place under a higher rate of sea-level rise (2–4 mm/yr – Hijma & Cohen, 2019).

Role of the backwater effect and tidal energy
Crevasses along the Old Rhine were directly driven by tidal backwater fluctuations in the estuary. These cause fluvial discharge to decrease or to

Table 5. Peat and its main properties.

Environment	Nutrient content	Water source	Salinity* (‰)	Water level relative to surface* (m)	Organic percentage‡	Stem density§
Phragmites marsh (reed)	Eutrophic	Groundwater-fed	<2; brackish to fresh†	−0.5 to −0.2 (tolerance for up to 1.7 m)	35 to 75%	High
Wood carr (alder, willow)	Eutrophic	Groundwater-fed	Fresh	−0.1 to +0.1	30 to 83%	Low
Sedge fen	Mesotrophic	Groundwater-fed	<1; brackish fresh to fresh	−0.3 to −0.1	76 to 92%	NA
Peat moss bog (*Sphagnum*)	Oligotrophic	Ombrotrophic	<0.1; fresh	+0.05 to +0.3	>69%	NA

* Den Held *et al.* (1992). † Salinity division after Van der Werff & Huls (1974), Table 1. ‡ Bos *et al.* (2012) for the Rhine-Meuse delta. § Boechat Albernaz *et al.* (2020).

stagnate, allowing sedimentation of either fluvial or marine sediments in the crevasses. The crevasses experience a reversing water level slope twice a day: during high water channel level is higher, during low water, floodbasin level is higher (especially when vegetation is sparse). The role of the backwater effect in forming the small crevasses (<2 km long) along the Old Rhine is evident from the increase in crevasse length towards the mouth (Fig. 8) and their absence upstream of the typical backwater length position (*ca* 30 km – cf. Van Dinter, 2013; De Haas *et al.*, 2019). This is because the backwater effect causes water levels in the channel to fluctuate more strongly towards the mouth, while water levels fluctuate less in the less connected floodbasins and are buffered by the swamp vegetation. Because of this, the channel-to-floodbasin water level gradient is also higher towards the mouth, leading to increasingly more efficient crevasse building when going downstream along the Old Rhine. A high slope from channel to floodbasin facilitates crevasses to remain open and grow (Slingerland & Smith, 1998). For the longer crevasses the slope effect is a less important mechanism, here seepage from the peat swamps and bogs probably helps to keep them open.

Over their Holocene lifetime, estuaries may experience variations in fluvial and tidal influence. From the Old Rhine case, three causes were identified behind tidal energy decrease over the lifetime of the estuary: (i) an increase in river discharge; (ii) coastal progradation; and (iii) estuary infilling. More river discharge leads to increased tidal dampening (Guo *et al.*, 2016; Braat *et al.*, 2017). As a result, discharge through crevasses occurs less often, eventually closing them off. Instead, overbank sediments now become mainly trapped in natural levées as observed in the model scenarios (Fig. 10; model 104). Along the Old Rhine, the increase in river discharge around *ca* 3800 cal BP resulted in less back-water driven crevasses while the fluvial levées became wider (Fig. 9). The opposite happened as river discharge decreased again from *ca* 2800 cal BP onwards. As a result, tidal flood and storm surges could probably penetrate more easily and further upstream. This may have led to (relatively coarse-grained) overbank deposition at sites *PB* and *VB*, up to 15 km from the mouth (Fig. 5B and D) (De Haas *et al.*, 2019). In addition, coastal progradation and estuary infilling likely contributed to a decrease in tidal energy along the Old Rhine during a decent portion of its lifetime. The former caused the estuary mouth to shift *ca* 10 km towards the west between 5700 and 3200 cal BP, as

waves kept transporting sand towards the coast (Van der Valk, 1995; De Haas *et al.*, 2019; Fig. 6). Also, progressive estuary infilling likely contributed to a decrease in tidal energy, when parallel channels closed and supratidal clays on estuarine channel and shoal sands were deposited in the most downstream 20 km between 3700 and 2700 cal BP (Figs 5C, 5D and 6). The above demonstrates that the relative importance of fluvial and marine processes may change in a non-linear way during the various stages of an estuary's life. Together with the strong steering effects of vegetation this results in complex morphology and facies architecture.

Implications for adaptation

This case study is relevant for deltas and coastal areas worldwide that are also facing increasing rates of relative sea-level rise and/or land subsidence. Due to its fast lateral expansion and biomass buildup, reed marsh generation fills up tidal basins effectively, which provides perspectives for land building. In deltas or coastal areas that face drowning due to (a combination of) subsidence or sea-level rise, reed marsh regeneration may be a feasible nature-based solution. Especially in cases where insufficient sediment is available to fill the entire coastal plain, reed growth may not only provide fast lateral infilling of shallow water areas, but it also sets in feedback mechanisms to help infill a basin (Fig. 11).

The Dutch coastal plain shows that a sea-level rise of 1 to 2 mm/yr (Old Rhine) up to 3 mm/yr (around 7 ka BP) slowly expands accommodation, while not dominantly forcing environmental changes, such as crevasse formation or changes in the composition of floodbasin vegetation. Future IPCC scenarios, however, predict rates of sea-level rise from 2.6 to 6.5 mm/yr (RCP 1–2.6) to 8.6 to 17 mm/yr (RCP 8.5) between 2080 to 2100 (Fox-Kemper *et al.*, 2021 – IPPC AR6; Ch9: table 9.10), which is up to an order of magnitude higher. In the western coastal plain of The Netherlands, similar rates have caused strong regression and drowning during the middle Holocene (Beets & Van der Spek, 2000; Vos, 2015). This means, that for most regions and scenarios of sea-level rise, additional adaptation measures are still required, for example, by sediment suppletion along the coast. For the Dutch situation, moreover, a large portion of the coastal plain is already several metres below current sea level, which is too low to facilitate peat accumulation. The property of reed to concentrate overbank sedimentation directly next to the

channel in levées may, however, still be useful for implementing nature-based solutions (Boechat Albernaz *et al.*, 2020). Such narrow sedimentation corridors may include embanked floodplains or shore-connected salt marshes, which may function as protective elements in coastal wetlands for the cases that cannot be fully filled with sediments or peat. Fluvial water is important in regulating these conditions, as freshwater and nutrient supply, but also regulating the water levels by dampening the tides. The Old Rhine case shows that fluvial discharge steered the type of flood basin vegetation – in turn affecting sedimentation dispersal patterns – while discharge variation may have caused varying degrees of tidal ingression.

In summary, vegetation can steer coastal evolution by enhanced land building, but with the expected rates of sea-level rise, boundary conditions will be expected to become more dominant while (managed) vegetation can still help adaptions combined with other measures.

CONCLUSIONS

This paper updates palaeoenvironmental reconstructions of the data-rich Old Rhine estuary, The Netherlands, to demonstrate that vegetation in coastal environments acts as a landscape builder and modulator. Over its lifetime, the system gradually evolved from a tidally-dominated basin into a peat-bounded tidal river. These results highlight that vegetation presence and composition not only is facilitated by morphology and hydrodynamics, but it also strongly steers sedimentary evolution of coastal plains and estuaries:

• Reed growth in tidal basins strongly steers sedimentary evolution of coastal plains and estuaries, though not simplistically by capturing sediment. Its growth reduces the tidal prism, contributing to the reduction in tidal range, in turn accelerating lateral reed accretion rates, further reducing the tidal prism. Subsequent *Phragmites* peat accumulation contributes to additional basin infilling. Our case shows that both of these effects strongly accelerate basin closure and terrestrialization.

• Rivers can create their own environment through affecting floodbasin vegetation: in Alder carrs, fed by river water nutrients, stem density is lower compared to reed marshes. Under these conditions, relatively wider levées and more frequent crevassing form, because water and sediment transport towards the floodbasins is easier.

• Secondary channels in wetlands may form under complex conditions. Facilitated by the hydrodynamics in wood carrs along the Old Rhine, tidal backwaters created small crevasses, by inducing frequent flow and sediment transport between channel and floodbasin. Longer creeks (>10 km) present at regular intervals along the Old Rhine channel belt served as hybrid bog drainage and fluvial/tidal floodwater crevasses.

• Over an estuary's life, the importance of fluvial and marine influence may strongly change resulting in complex morphology and facies architecture. This is exemplified by the development of wider natural levées, as tidal influence on the Old Rhine decreased around 3800 cal BP – after progressive lower estuary infilling and fluvial discharge increase.

Our results have implications for this wetland archaeology hotspot and for future wetland management, especially in broad lowland coastal plains:

• Since the Late Neolithic, wood carrs and tidal backwater effects facilitated creek formation and hence water route connectivity. The creek levées provided higher places to live until groundwater level rise caused them to be overgrown by peat after several centuries to millennia. After the Bronze Age, crevasse sedimentation decreased and, probably around Roman times, a decent portion of them was overgrown by peat, making them much less suited for habitation. Although sedimentation on their levées had decreased, many creeks possibly still had open channels suited for navigation for a much longer period.

• For future coastal management, our results may help to mitigate land loss in coastal wetlands under accelerating sea-level rise. Reed demonstrates to be a very effective basin filler, not only because it catches sediment but especially due to feedbacks it can set in that have the potential to eventually close basins. Reed is suitable because it expands laterally, even under brackish conditions, reducing tidal prism to promote tidal basin infilling. Our case shows that peat growth can keep up with lower rates of sea-level rise if initial water conditions are shallow and remain brackish to fresh.

ACKNOWLEDGEMENTS

DATA AVAILABILITY STATEMENT

The data that supports the findings of this study are available in the supplementary material of this article.

REFERENCES

ABR (1992) *Het Archeologisch Basis Register (ABR).* https://docplayer.nl/23515946-Het-archeologisch-basisregister-abr-versie-1-0-november-1992.html

Abrahamse, J.E., **Kosian, M.C.**, **Rutte, R.**, **Diesfeldt, O.**, **Pané, I.**, **van Mil, Y.** and **de Waaijer, A.** (2021) *Watersysteem en stadsvorm in Holland: Een verkenning in kaartbeelden: 1575, 1680, 1900 en 2015*, pp. 47–121. OverHolland, Rotterdam, The Netherlands.

Adams, P.N., **Slingerland, R.L.** and **Smith, N.D.** (2004) Variations in natural levee morphology in anastomosed channel flood plain complexes. *Geomorphology*, **61**(142), 127.

Allen, J.R.L. (1990) The formation of coastal peat marshes under an upward tendency of relative sea-level. *J. Geol. Soc. London*, **147**, 743–745.

Allen, J.R.L. (2000) Morphodynamics of Holocene salt marshes: a review sketch from the Atlantic and Southern North Sea coasts of Europe. *Quatern. Sci. Rev.*, **19**(12), 1155–1231.

Baeteman, C. (1999) The Holocene depositional history of the IJzer palaeovalley (Western Belgian coastal plain) with reference to the factors controlling the formation of intercalated peat beds. *Geol. Belgica*, **2**(3–4), 39–72.

Bakker, M. and **Van Smeerdijk, D.G.** (1982) A palaeoecological study of a late Holocene section from "het Ilperveld", Western Netherlands. *Rev. Palaeobot. Palynol.*, **36**, 95–163.

Batterbee, R.W., **Jones, V.J.**, **Flower, R.J.**, **Cameron, N.G.**, **Bennion, H.**, **Carvalho, L.** and **Juggins, S.** (2001) Diatoms. In: *Chapter 8: Tracking Environmental Change Using Lake Sediments Volume 3: Terrestrial, Algal and Siliceous Indicators* (Eds Smol, J.P., Birks, H.J.B. and Last, W.M.), pp. 150–202. Kluwer Academic Publishers, Dordrecht.

Beets, D.J., **De Groot, T.A.M.** and **Davies, H.A.** (2003) Holocene tidal back-barrier development at decelerating sea-level rise: a 5 millennia record, exposed in the western Netherlands. *Sediment. Geol.*, **158**(1–2), 117–144.

Beets, D.J., **Roep, T.B.** and **Westerhoff, W.E.** (1996) The Holocene Bergen Inlet: closing history and related barrier progradation. *Mededelingen Rijks Geologische Dienst*, **57**, 97–131.

Beets, D.J. and **Van der Spek, A.J.F.** (2000) The Holocene evolution of the barrier and the back-barrier basins of Belgium and the Netherlands as a function of late Weichselian morphology, relative sea-level rise and sediment supply. *Neth. J. Geosci.*, **79**(1), 3–16.

Beets, D.J., **Van der Valk, L.** and **Stive, M.J.F.** (1992) Holocene evolution of the coast of Holland. *Mar. Geol.*, **103**, 423–443.

Behre, K.-E. (2004) Coastal development, sea-level change and settlement history during the later Holocene in the Clay District of Lower Saxony (Niedersachsen), northern Germany. *Quat. Int.*, **112**, 37–53.

Behre, K.-E. (2007) A new Holocene sea-level curve for the southern North Sea. *Boreas*, **36**(1), 82–102.

Bennema, J. and **Van der Meer, K.** (1952) De genese van Walcheren. In: *Boor & Spade*, pp. 245–255. N.V. A. Oosthoek's Uitgeverij MIJ., Utrecht, The Netherlands.

Berendsen, H.J.A. (1982) *De genese van het landschap in het zuiden van de provincie Utrecht.* Utrecht University, Utrecht.

Berendsen, H.J.A. and **Stouthamer, E.** (2000) Late Weichselian and Holocene palaeogeography of the Rhine–Meuse delta, The Netherlands. *Palaeogeogr. Palaeoclimatol. Palaeoecol.*, **161**(3–4), 311–335.

Blom, E. and **Roessingh, W.** (2007) Aan de rand van het Romeinse Rijk, archeologisch onderzoek in de Munnikenpolder te Leiderdorp. *ADC-rapport 802 (Amersfoort)*, 82 pp.

Boechat Albernaz, M., **Roelofs, L.**, **Pierik, H.J.** and **Kleinhans, M.G.** (2020) Natural levee evolution in vegetated fluvial-tidal environments. *Earth Surf. Process. Landf.*, **45**(15), 3824–3841.

Borger, G. J. (1992) Draining—digging—dredging; the creation of a new landscape in the peat areas of the low countries. In: *Fens and Bogs in The Netherlands: Vegetation, History, Nutrient Dynamics and Conservation* (Ed. Verhoeven, J.T.A.), pp. 131–171. Springer, Dordrecht.

Bos, I.J., **Busschers, F.S.** and **Hoek, W.Z.** (2012) Organic-facies determination: a key for understanding facies distribution in the basal peat layer of the Holocene Rhine-Meuse delta, The Netherlands. *Sedimentology*, **59**(2), 676–703.

Bos, I.J., **Feiken, H.**, **Bunnik, F.** and **Schokker, J.** (2009) Influence of organics and clastic lake fills on distributary channel processes in the distal Rhine–Meuse delta (The Netherlands). *Palaeogeogr. Palaeoclimatol. Palaeoecol.*, **284**(374), 355.

Bos, I.J. and **Stouthamer, E.** (2011) Spatial and temporal distribution of sand-containing basin fills in the holocene rhine-meuse delta, the Netherlands. *J. Geol.*, **119**(6), 641–660.

Bosch, J.H.A. and **Pruissers, A.P.** (1979) *De laatste 4500 jaar Rijn bij Leiden*, pp. 25–36. Jaarverslag archeol. begel. cie, Leiden.

Braat, L., **Van Kessel, T.**, **Leuven, J.R.** and **Kleinhans, M.G.** (2017) Effects of mud supply on large-scale estuary

morphology and development over centuries to millennia. *Earth Surf. Dyn.*, **5**(4), 617–652.

Branch, N.P., **Batchelor, C.R.**, **Cameron, N.G.**, **Coope, G.R.**, **Densem, R.**, **Gale, R.**, **Green, C.** and **Williams, A.N.** (2012) Holocene environmental changes in the Lower Thames Valley, London, UK: implications for understanding the history of Taxus woodland. *Holocene*, **22**, 1143–1158.

Brew, D.S., **Horton, B.P.**, **Evans, G.**, **Innes, J.B.** and **Shennan, I.** (2015) Holocene sea-level history and coastal evolution of the north-western Fenland, eastern England. *Proc. Geol. Assoc.*, **126**(1), 72–85.

Brierley, G.J., **Ferguson, R.J.** and **Woolfe, K.J.** (1997) What is a fluvial levee? *Sediment. Geol.*, **114**(1–4), 1–9.

Bronk Ramsey, C. and **Lee, S.** (2013) Recent and planned developments of the program OxCal. *Radiocarbon*, **55**(2–3), 720–730.

Brückner, M.Z.M., **Braat, L.**, **Schwarz, C.** and **Kleinhans, M.G.** (2020) What came first, mud or biostabilizers? Elucidating interacting effects in a coupled model of mud, saltmarsh, microphytobenthos, and estuarine morphology. *Water Resour. Res.*, **56**, e2019WR026945.

Brückner, M.Z.M., **Schwarz, C.**, **van Dijk, W.M.**, **van Oorschot, M.**, **Douma, H.** and **Kleinhans, M.G.** (2019) Salt marsh establishment and eco-engineering effects in dynamic estuaries determined by species growth and mortality. *J. Geophys. Res. Earth*, **124**, 2962–2986.

Cattaneo, A. and **Steel, R.J.** (2003) Transgressive deposits: a review of their variability. *Earth-Sci. Rev.*, **62**(3–4), 187–228.

Clement, A.J.H., **Fuller, I.C.** and **Sloss, C.R.** (2017) Facies architecture, morphostratigraphy, and sedimentary evolution of a rapidly-infilled Holocene incised-valley estuary: The lower Manawatu valley, North Island New Zealand. *Mar. Geol.*, **390**, 214–233.

Cleveringa, J. (2000) *Reconstruction and Modelling of Holocene Coastal Evolution of the Western Netherlands*. Universiteit Utrecht, Utrecht.

Coco, G., **Zhou, Z.**, **van Maanen, B.**, **Olabarrieta, M.**, **Tinoco, R.** and **Townend, I.** (2013) Morphodynamics of tidal networks: Advances and challenges. *Mar. Geol.*, **346**, 1–16.

Cohen, K.M., **Stouthamer, E.**, **Hoek, W.Z.**, **Berendsen, H.J.A.** and **Kempen, H.F.J.** (2009) Zand in banen - zanddieptekaarten van het Rivierengebied en het IJsseldal in de provincies Gelderland en Overijssel.

Cohen, K.M., **Stouthamer, E.**, **Pierik, H.J.** and **Geurts, A.H.** (2012) Digitaal Basisbestand Palaeogeografie van de Rijn-Maas Delta/Rhine-Meuse Delta Studies. In: *Digital Basemap for Delta Evolution and Palaeogeography*. Rhine-Meuse Delta Studies, Dept. Fysische Geografie, Universiteit Utrecht, Utrecht, The Netherlands.

Cooper, J.A.G., **Jackson, D.W.T.**, **Dawson, A.G.**, **Dawson, S.**, **Bates, C.R.** and **Ritchie, W.** (2012) Barrier islands on bedrock: A new landform type demonstrating the role of antecedent topography on barrier form and evolution. *Geology*, **40**(10), 923–926.

Coops, H., **Geilen, N.** and **Van der Velde, G.** (1994) Distribution and growth of the helophyte species Phragmites australis and Scirpus lacustris in water depth gradients in relation to wave exposure. *Aquat. Bot.*, **48**, 273–284.

D'Alpaos, A., **Lanzoni, S.**, **Mudd, S.M.** and **Fagherazzi, S.** (2006) Modeling the influence of hydroperiod and vegetation on the cross-sectional formation of tidal channels. *Estuar. Coast. Shelf Sci.*, **69**(324), 311.

Davis, R.A., Jr. and **Clifton, H.E.** (1987) Sea-level change and the preservation potential of wave-dominated and tide-dominated coastal sequences. *Soc. Econom. Palaeontol. Mineral.*

De Bakker, H. and **Schelling, J.** (1966) Systeem van bodemclassificatie voor Nederland: de hogere niveaus.

De Bruin, J., **Hessing, W.** and **Noordervliet, J.** (2022) Hazerswoude. Een ontbrekende schakel in de limes?. *Archeobrief*, **6**(1), 16–21.

De Haas, T., **Pierik, H.J.**, **van der Spek, A.J.F.**, **Cohen, K.M.**, **van Maanen, B.** and **Kleinhans, M.G.** (2018) Holocene evolution of tidal systems in The Netherlands: Effects of rivers, coastal boundary conditions, eco-engineering species, inherited relief and human interference. *Earth-Sci. Rev.*, **177**, 139–163.

De Haas, T., **van der Valk, L.**, **Cohen, K.M.**, **Pierik, H.J.**, **Weisscher, S.A.H.**, **Hijma, M.P.**, **van der Spek, A.J.F.** and **Kleinhans, M.G.** (2019) Long-term evolution of the Old Rhine estuary: unraveling effects of changing boundary conditions and inherited landscape. *Deposition. Rec.*, **5**, 84–108.

De Jong, J. (1977) Uitkomsten van C14-ouderdomsbepalingen aan boringen uit het Oude Rijn-gebied. *TNO-Report*, **800**, 7.

De Wolf, H. (1981) Diatomeeënonderzoek van de boring Zuid plaspolder. *TNO-Report 425*.

De Wolf, H. (1986a) Diatomeeënonderzoek van de boring Schipluiden I. *TNO-Report 480*.

De Wolf, H. (1986b) Diatomeeënonderzoek van de boring Schipluiden II. *TNO-Report 481*.

De Wolf, H. and **Cleveringa, P.** (2006) Diatoms. Schipluiden, a Neolithic Settlement on the Dutch North Sea Coast c 3500.

Deegan, B.M., **White, S.D.** and **Ganf, G.G.** (2007) The influence of water level fluctuations on the growth of four emergent macrophyte species. *Aquat. Bot.*, **86**, 309–315.

Deforce, K. (2011) Middle and late Holocene vegetation and landscape evolution of the Scheldt estuary: a palynological study of a peat deposit from Doel (Belgium). *Geologica Belgica*, **14**(3–4), 277–288.

Deltares. (2017) *Delft3d-Flow: Simulation of Multi-Dimensional Hydrodynamic Flows and Transport Phenomena, Including Sediments: User Manual*. Deltares, Delft.

Den Held, A.J., **Schmitz, M.** and **Van Wirdum, G.** (1992) Types of terrestrializing fen vegetation in the Netherlands. In: *Fens and Bogs in the Netherlands* (Ed. Verhoeven, J.), pp. 237–321. Springer, Dordrecht.

Denys, L. (1989) Observations on the transition from Calais deposits to surface peat in the western Belgian coastal plain: Results of a palaeoenvironmental diatom study. In: *Quaternary Sea-Level Investigations from Belgium. Professional paper Belgische Geologische Dienst* (Ed. Baeteman, C.), Vol. **241**, pp. 20–43. Geological survey of Belgium, Brussels.

Devoy, R.J.N. (1979) Flandrian sea level changes and vegetational history of the Lower Thames Estuary. *Philos. Transac. R. Soc. London*, **B285**, 355–407.

Diependaele, S. and **Drenth, E.** (2010) Archeologisch Onderzoek langs de Rijksweg N11 (Spookverlaat) ten behoeve van de Aanleg van het Windturbinepark Rijnwoud te Hazerswoude-Rijndijk (gem. Rijnwoude, prov. Zuid-Holland): Een Neolithische Vindplaats langs de Oude Rijn. *ArcheoMedia Rapport A06-286-R*.

Engloner, A.I. (2009) Structure, growth dynamics and biomass of reed (Phragmites australis) - A review. *Flora: Morphol. Distrib. Funct. Ecol. Plants*, **204**(5), 331–346.

Erkens, G. and **Cohen, K.M.** (2009) Quantification of intra-Holocene sedimentation in the Rhine-Meuse delta: a record of variable sediment delivery. In: *Sediment*

Dynamics in the Rhine Catchment (Ed. Erkens, G.), pp. 117–172. PhD Thesis Utrecht University. Utrecht.

Fagherazzi, S., **Kirwan, M.L.**, **Mudd, S.M.**, **Guntenspergen, G.R.**, **Temmerman, S.**, **D'Alpaos, A.** and **Clough, J.** (2012) Numerical models of salt marsh evolution: Ecological, geomorphic, and climatic factors. *Rev. Geophys.*, **50**(1).

Fox-Kemper, B., **Hewitt, H.T.**, **Xiao, C.**, **Aðalgeirsdóttir, G.**, **Drijfhout, S.S.**, **Edwards, T.L.**, **Golledge, N.R.**, **Hemer, M.**, **Kopp, R.E.**, **Krinner, G.**, **Mix, A.**, **Notz, D.**, **Nowicki, S.**, **Nurhati, I.S.**, **Ruiz, L.**, **Sallée, J.-B.**, **Slangen, A.B.A.** and **Yu, Y.** (2021) Ocean, cryosphere and sea level change. In: *Climate Change 2021: The Physical Science Basis Contribution of Working Group I to the Sixth Assessment Report of the Intergovernmental Panel on Climate Change*, pp. 1211–1362. Cambridge University Press, Cambridge and New York, NY. https://doi.org/10.1017/9781009157896.011.

Fruergaard, M., **Andersen, T.J.**, **Nielsen, L.H.**, **Johannessen, P.N.**, **Aagaard, T.** and **Pejrup, M.** (2014) High-resolution reconstruction of a coastal barrier system: Impact of Holocene sea-level change. *Sedimentology*, **62**(3), 928–969.

Godwin, H. (1943) Coastal peat beds of the British Isles and North Sea: Presidential address to the british ecological society 1943. *J. Ecol.*, **31**(2), 199.

Gouw, M.J.P. and **Erkens, G.** (2007) Architecture of the Holocene Rhine-Meuse delta (the Netherlands) – A result of changing external controls. *Neth. J. Geosci. Geologie en Mijnbouw*, **86**(1), 23–54.

Guo, L., **van der Wegen, M.**, **Wang, Z.B.**, **Roelvink, D.** and **He, Q.** (2016) Exploring the impacts of multiple tidal constituents and varying river flow on long-term, large-scale estuarine morphodynamics by means of a 1-D model. *Case Rep. Med.*, **121**, 1000–1022.

Hamilton, C.A., **Kirby, J.R.**, **Lane, T.P.**, **Plater, A.J.** and **Waller, M.P.** (2019) Sediment supply and barrier dynamics as driving mechanisms of Holocene coastal change for the southern North Sea basin. *Quat. Int.*, **500**, 147–158.

Hassan, G.S., **Espinosa, M.A.** and **Isla, F.I.** (2006) Modern diatom assemblages in surface sediments from estuarine systems in the southeastern Buenos Aires Province, Argentina. *J. Palaeolimnol.*, **35**, 39–53.

Havinga, A.J. and **Van den Berg van Saparoea, R.** (1982) Vegetational development of a wood peat deposit as read from its pollen content. In: *Proceedings of the Symposium On Peat Lands Below Sea Level: Peat Lands Lying Below Sea Level In The Western Part Of The Netherlands, Their Geology, Reclamation, Soils, Management And Land Use* (Eds de Bakker, H. and van den Berg, M.W.), pp. 275–281. International Institute for Land Reclamation and Improvement, Wageningen.

Heiri, O., **Lotter, A.** and **Lemke, G.** (2001) Loss on ignition as a method for estimating organic and carbonate content in sediments: reproducibility and comparability of results. *J. Palaeolimnol.*, **25**, 101–110.

Hendrikx, P. (1983) Rijn en Maas: landschap en bewoning van de Romeinse tijd tot ca. 1000. PHD Thesis, University of Amsterdam, Amsterdam.

Hijma, M.P. and **Cohen, K.M.** (2011) Holocene transgression of the Rhine river mouth area, The Netherlands/Southern North Sea: palaeogeography and sequence stratigraphy. *Sedimentology*, **58**(6), 1453–1485.

Hijma, M.P. and **Cohen, K.M.** (2019) Holocene sea-level database for the Rhine-Meuse Delta, The Netherlands: Implications for the pre-8.2 ka sea-level jump. *Quatern. Sci. Rev.*, **214**, 68–86.

Hijma, M.P., **Cohen, K.M.**, **Hoffmann, G.**, **Van der Spek, A.J.F.** and **Stouthamer, E.** (2009) From river valley to estuary: the evolution of the Rhine mouth in the early to middle Holocene (western Netherlands, Rhine-Meuse delta). *Neth. J. Geosci.*, **88**(1), 13–53.

Hoffmann, T., **Erkens, G.**, **Cohen, K.M.**, **Houben, P.**, **Seidel, J.** and **Dikau, R.** (2007) Holocene floodbasin sediment storage and hillslope erosion within the Rhine catchment. *Holocene*, **17**(1), 105–118.

Hudson, P.F. and **Heitmuller, F.T.** (2003) Local- and watershed-scale controls on the spatial variability of natural levee deposits in a large fine-grained floodbasin: Lower Punico Basin, Mexico. *Geomorphology*, **56**(3–4), 255–269.

Jansma, E. (2020) Hydrological disasters in the NW-European Lowlands during the first millennium AD: a dendrochronological reconstruction. *Netherlands Journal of Geosciences*, **99**, E11.

Jarrett, J.T. (1976) Tidal prism – inlet area relationships.

Jelgersma, S., **Stive, M.J.F.** and **Van der Valk, L.** (1995) Holocene storm surge signatures in the coastal dunes of the western Netherlands. *Mar. Geol.*, **125**, 95–110.

Kleinhans, M.G., **Cohen, K.M.**, **Hoekstra, J.** and **Ijmker, J.M.** (2011) Evolution of a bifurcation in a meandering river with adjustable channel widths, Rhine delta apex, The Netherlands. *Earth Surf. Process. Landf.*, **36**(15), 2011–2027.

Kleinhans, M.G., **de Vries, B.**, **Braat, L.** and **van Oorschot, M.** (2018) Living landscapes: Muddy and vegetated floodbasin effects on fluvial pattern in an incised river. *Earth Surf. Process. Landf.*, **43**(14), 2948–2963.

Kleinhans, M.G., **Roelofs, L.**, **Weisscher, S.A.H.**, **Lokhorst, I.R.** and **Braat, L.** (2022) Estuarine morphodynamics and development modified by floodplain formation. *Earth Surf. Dyn.*, **10**(2), 367–381.

Kooistra, L.I., **van Dinter, M.**, **Dütting, M.K.**, **Van Rijn, P.** and **Cavallo, C.** (2013) Could the local population of the Lower Rhine delta supply the Roman army? Part 1: The archaeological and historical framework. *J. Archaeol. Low Countries*, **4**(2), 5–23.

Koster, K., **Stafleu, J.** and **Cohen, K.M.** (2016) Generic 3D interpolation of Holocene base-level rise and provision of accommodation space, developed for the Netherlands coastal plain and infilled palaeovalleys. *Basin Res.*, **29**(6), 1–23.

Kroes, R.A.C. and **Feiken, H.** (2011) Plangebied Polder Nieuwkoop, Zuid- en Noordeinderpolder, gemeente Alphen aan den Rijn; archeologisch vooronderzoek: een beleidsadvieskaart. *RAAP-Report* 2468, Weesp, the Netherlands.

Kuipers, S.F. (1960) *Een bijdrage tot de kennis van de bodem van Schouwen-Duiveland en Tholen naar de toestand vóór 1953*. Centrum voor Landbouwpublicaties en Landbouwdocumentatie (PUDOC). Report Wageningen University, Wageningen.

Lenselink, G. (1988). Valkenburg aan de Oude Rijn in de Romeinse tijd: landschapsreconstructie gebaseerd op electro-magnetische geleidbaarheidsmetingen, bodemprofielen, opgravingsgegevens en allerhande kaartmateriaal. Unpublished report Wageningen University.

Lesser, G., **Roelvink, J.**, **van Kester, J.** and **Stelling, G.** (2004) Development and validation of a three-dimensional morphological model. *Coastal Eng.*, **51**(8), 883–915.

Lissner, J. and **Schierup, H.-H.** (1997) Effects of salinity on the growth of Phragmites australis. *Aquat. Bot.*, **55**, 247–260.

Lokhorst, I., **Braat, L.**, **Leuven, J.R.F.W.**, **Baar, A.**, **van Oorschot, M.**, **Selaković, S.** and **Kleinhans, M.G.** (2018)

Morphological effects of vegetation on the tidal–fluvial transition in holocene estuaries. *Earth Surf. Dyn.*, **6**(4), 883–901.

Long, A.J., Scaife, R.G. and Edwards, R.J. (2000) Stratigraphic architecture, relative sea-level, and models of estuary development in southern England: New data from Southampton Water. *Geol. Soc. Spec. Pub.*, **175**, 253–279.

Long, A.J., Waller, M.P.P. and Stupples, P. (2006) Driving mechanisms of coastal change: Peat compaction and the destruction of late Holocene coastal wetlands. *Mar. Geol.*, **225**(1–4), 63–84.

Makaske, B. (1998) *Anastomosing Rivers. Forms, Processes and Sediments.* Utrecht University, Utrecht.

Makaske, B., Berendsen, H.J.A. and van Ree, M.H.M. (2007) Middle Holocene Avulsion-Belt Deposits in the Central Rhine-Meuse Delta, The Netherlands. *J. Sediment. Res.*, **77**, 110–123.

Makaske, B., Smith, D.G. and Berendsen, H.J.A. (2002) Avulsions, channel evolution and floodbasin sedimentation rates of the anastomosing upper Columbia River, British Columbia, Canada. *Sedimentology*, **49**(5), 1049–1071.

Marco-Barba, J., Burjachs, F., Reed, J.M., Santisteban, C., Usera, J.M., Alberola, C., Expósito, I., Guillem, J., Patchett, F., Vicente, E., Mesquita-Joanes, F. and Miracle, M.R. (2019) Mid-Holocene and historical palaeoecology of the Albufera de València coastal lagoon. *Limnetica*, **38**(1), 353–389.

McMahon, W.J. and Davies, N.S. (2018) The shortage of geological evidence for pre-vegetation meandering rivers. Fluvial meanders and their sedimentary products in the rock record. In: *Fluvial Meanders and Their Sedimentary Products in the Rock Record* (Eds Ghinassi, M., Colombera, L., Mountney, N.P. and Reesink, A.J.H.), pp. 119–148. Wiley-Blackwell, Hoboken, NJ.

Meijer, Y., Wilbers, A.W.E., Moerman, S. and Torremans, R.P.B. (2020) Wassenaar aan den Rijn, Bewoning in een rivierenlandschap van de Bronstijd tot de Nieuwe tijd. *IDDS Archaeol. Rapp.*, **2336**, 358.

Millard, C., Hajek, E. and Edmonds, D.A. (2017) Evaluating controls on crevasse-splay size: implications for floodbasin-basin filling. *J. Sediment. Res.*, **87**(7), 722–739.

Nichol, S.L. (1991) Zonation and sedimentology of estuarine facies in an incised valley, wave-dominated, microtidal setting, New South Wales, Australia.

Nienhuis, J.H., Törnqvist, T.E. and Esposito, C.R. (2018) Crevasse splays versus avulsions: A recipe for land building with levee breaches. *Geophys. Res. Lett.*, **45**(9), 4058–4067.

Pierik, H.J., Cohen, K.M., Vos, P.C., van der Spek, A.J.F. and Stouthamer, E. (2017) Late Holocene coastal-plain evolution of the Netherlands: the role of natural preconditions in human-induced sea ingressions. *Proc. Geol. Assoc.*, **128**(2), 180–197.

Pierik, H.J., Stouthamer, E. and Cohen, K.M. (2017) Natural levee evolution in the Rhine-Meuse delta, the Netherlands, during the first millennium CE. *Geomorphology*, **295**, 215–234.

Pierik, H.J., Stouthamer, E., Schuring, T. and Cohen, K.M. (2018) Human-caused avulsion in the Rhine-Meuse delta before historic embankment (The Netherlands). *Geology*, **46**(11), 935–938.

Pons, L.J. (1992) Holocene peat formation in the lower parts of the Netherlands. In: *Fens and Bogs in The Netherlands: Vegetation, History, Nutrient Dynamics and Conservation* (Ed. Verhoeven, J.T.A.), pp. 7–79. Springer, Dordrecht.

Pons, L.J., Jelgersma, S., Wiggers, A.J. and De Jong, J. (1963) Evolution of the Netherlands coastal area during the Holocene. In: *Verhandelingen van het KNGMG "Transactions of the Jubilee Convention - Part Two"* (Ed. de Jong, J.), pp. 197–207. Koninklijk Nederlands Geologisch Mijnbouwkundig Genootschap, Gravenhave.

Pons, L.J. and Wiggers, A.J. (1959) De Holocene wordingsgeschiedenis van Noordholland en het Zuiderzee gebied.

Raven, J.G.M. and Kuijper, W.J. (1981) Calais deposits (Holocene) near Benthuizen (Province of Zuid-Holland, the Netherlands), with a palaeoecological reconstruction. *Mededelingen van de Werkgroep voor Tertiaire en Kwartaire Geologie*, **18**(1), 11–28.

Redfield, A.C. (1965) Ontogeny of a salt marsh estuary. *Science*, **147**(3653), 50–55.

Reijers, V.C., van den Akker, M., Cruijsen, P.M., Lamers, L.P. and van der Heide, T. (2019) Intraspecific facilitation explains the persistence of Phragmites australis in modified coastal wetlands. *Ecosphere*, **10**(8).

Reimer, P.J., Austin, W.E.N., Bard, E., Bayliss, A., Blackwell, P.G., Bronk Ramsey, C., Butzin, M., Cheng, H., Edwards, R.L., Friedrich, M., Grootes, P.M., Guilderson, T.P., Hajdas, I., Heaton, T.J., Hogg, A.G., Hughen, K.A., Kromer, B., Manning, S.W., Muscheler, R., et al. (2020) The IntCal20 Northern Hemisphere Radiocarbon Age Calibration Curve (0–55 cal kBP). *Radiocarbon*, **62**(4), 725–757.

Renberg, I. (1990) A procedure for preparing large sets of diatom slides from sediment cores. *J. Palaeolimnol.*, **4**(1), 87–90.

Roeleveld, W. (1974) The Holocene Evolution of the Groningen Marine-Clay District. *Berichten van de Rijksdienst voor het Oudheidkundig Bodemonderzoek*, **24**, 1–133.

Roep, T.B., Van der Valk, L. and Beets, D.J. (1991) Strandwallen en zeegaten langs de Hollandse kust. *Grondboor Hamer*, **45**, 115–124.

Rooth, J.E. and Stevenson, J.C. (2000) Sediment deposition patterns in Phragmites australis communities: Implications for coastal areas threatened by rising sea-level. *Wetlands Ecol. Manag.*, **8**(2), 173–183.

Roy, P.S., Thom, B.G. and Wright, L.D. (1980) Holocene sequences on an embayed high-energy coast: an evolutionary model. *Sediment. Geol.*, **26**(1–3), 1–19.

Savenije, H.H.G. (2015) Prediction in ungauged estuaries: An integrated theory. *Water Resour. Res.*, **51**, 2464–2476.

Sawai, Y., Horton, B.P., Kemp, A.C., Hawkes, A.D., Nagumo, T. and Nelson, A.R. (2018) Relationships between diatoms and tidal environments in Oregon and Washington, USA. *Diatom Res.*, **31**(1), 17–38.

Sawai, Y., Nasu, H. and Yasuda, Y. (2002) Fluctuations in relative sea-level during the past 3000 yr in the Onnetoh estuary, Hokkaido, northern Japan. *J. Quatern. Sci.*, **17**(5–6), 607–622.

Schepers, L., Van Braeckel, A., Bouma, T.J. and Temmerman, S. (2020) How progressive vegetation die-off in a tidal marsh would affect flow and sedimentation patterns: A field demonstration. *Limnol. Oceanogr.*, **65**(2), 401–412.

Schoeneberger, P.J., Wysocki, D.A., Benham, E.C. and Broderson, W.D. (1998) *Fieldbook for Describing and Sampling Soils. Version 1.1*, p. 182. National Soil Survey Center, National Resources Conservation Service, U.S. Department of Agriculture, Lincoln, Nebraska.

Slingerland, R. and Smith, N.D. (1998) Necessary conditions for a meandering-river avulsion. *Geology*, **26**(5), 435–438.

Smith, D.E., **Harrison, S.**, **Firth, C.R.** and **Jordan, J.T.** (2011) The early Holocene sea level rise. *Quatern. Sci. Rev.*, **30** (15–16), 1846–1860.

Smith, N.D. and **Pérez-Arlucea, M.** (2004) Effects of peat on the shapes of alluvial channels: examples from the Cumberland Marshes, Saskatchewan, Canada. *Geomorphology*, **61**(3–4), 323–335.

Smith, N.D., **Slingerland, R.L.**, **Pérez-Arlucea, M.** and **Morozova, G.S.** (1998). The 1870s avulsion of the Saskatchewan River. *Can. J. Earth Sci.*, **35**(4), 453–466.

Soil Survey Staff (2010) *Keys to Soil Taxonomy*, 11th edn. USDA Natural Resources Conservation Service, Washington, DC.

Stanley, D.J. and **Warne, A.G.** (1994) Worldwide initiation of holocene marine deltas by deceleration of sea-level rise. *Science*, **265**(5169), 228–231.

Stouthamer, E. (2001) Sedimentary products of avulsions in the Holocene Rhine–Meuse Delta, The Netherlands. *Sediment. Geol.*, **145**(1–2), 73–92.

Stouthamer, E. and **Berendsen, H.J.A.** (2001) Avulsion frequency, avulsion duration, and interavulsion period of holocene channel belts in the Rhine-Meuse delta, The Netherlands. *J. Sediment. Res.*, **71**(4), 589–598.

Stouthamer, E., **Cohen, K.M.** and **Gouw, M.J.P.** (2011) Avulsion and its implications for fluvial-deltaic architecture: Insights from the Holocene Rhine-Meuse Delta. In: *From River to Rock Record: The Preservation of Fluvial Sediments and their Subsequent Interpretation* (Eds Davidson, S.K., Leleu, S. and North, C.P.), Vol. **97**, pp. 215–231. Society for Sedimentary Geology, Special Publication, Tulsa, Oklahoma.

STOWA. (2014) Handboek hydrobiologie, Hoofdstuk 9: Kiezelwieren. Including Werkvoorschrift.

Temmerman, S., **Bouma, T.J.**, **Van de Koppel, J.**, **Van der Wal, D.**, **De Vries, M.B.** and **Herman, P.M.J.** (2007) Vegetation causes channel erosion in a tidal landscape. *Geology*, **35**(7), 631–634.

TNO-GSN (2022) *TNO-Geological Survey of the Netherlands.* Stratigrafische Nomenclator van Nederland, Utrecht. Available at. http://www.dinoloket.nl/stratigrafische-nomenclator/.

Tol, A.J. and **Jansen, B.** (2012) Sleuven door de delta van de Oude Rijn. *Archol Rapport*, **172**, 388.

Toonen, W.H.J., **Donders, T.H.**, **Van der Meulen, B.**, **Cohen, K.M.** and **Prins, M.A.** (2013) A composite Holocene palaeolood chronology of the Lower Rhine. In: *A Holocene Lood Record of the Lower Rhine*, pp. 137–150. PhD thesis, Utrecht University, Utrecht.

Toonen, W.H.J., **Foulds, S.A.**, **Macklin, M.G.** and **Lewin, J.** (2017) Events, episodes, and phases: Signal from noise in flood-sediment. *Geology*, **45**(4), 331–334.

Tooth, S. (1999) Downstream changes in floodbasin character on the Northern Plains of arid central Australia. *Fluvial Sedimentol VI*, **28**, 93–112.

Tooth, S. (2005) Splay formation along the lower reaches of ephemeral rivers on the Northern Plains of arid central Australia. *J. Sediment. Res.*, **75**(4), 636–649.

Törnqvist, T.E. and **Van Dijk, G.J.** (1993) Optimizing sampling strategy for radiocarbon dating of Holocene fluvial systems in a vertically aggrading setting. *Boreas*, **22** (2), 129–145.

Umitsu, M., **Buman, M.**, **Kawase, K.** and **Woodroffe, C.D.** (2001) Holocene palaeoecology and formation of the shoalhaven river deltaic-estuarine plains, southeast australia. *Holocene*, **11**(4), 407–418.

Van Asch, N. (2007) *Palaeo Seepage in the Holocene Subsurface Near Woerden, Central Netherlands.* MSc Thesis. Utrecht University/Vrije Universiteit Amsterdam, Utrecht/Amsterdam.

Van Asselen, S. (2011) The contribution of peat compaction to total basin subsidence: implications for the provision of accommodation space in organic-rich deltas. *Basin Res.*, **23**(2), 239–255.

Van Asselen, S., **Erkens, G.**, **Stouthamer, E.**, **Woolderink, H.A.**, **Geeraert, R.E.** and **Hefting, M.M.** (2018) The relative contribution of peat compaction and oxidation to subsidence in built-up areas in the Rhine-Meuse delta, The Netherlands. *Sci. Total Environ.*, **636**, 177–191.

Van Asselen, S., **Stouthamer, E.** and **Van Asch, T.W.J.** (2009) Effects of peat compaction on delta evolution: A review on processes, responses, measuring and modeling. *Earth-Sci. Rev.*, **92**(1–2), 35–51.

Van de Ven, G.P. (1993) *Leefbaar Laagland.* Geschiedenis van de waterbeheersing en landaanwinning in Nederland, Matrijs, Utrecht.

Van der Leije, J. and **Hamburg, T.** (2014) Archaeologisch onderzoek naar de geschiedenis van Katwijk aan Zee, Inventariserend Veldonderzoek – proefsleuven Kustversterking Katwijk (Z.H.). *Archol Rap.*, **209**, 100.

Van der Molen, J. and **de Swart, H.E.** (2001a) Holocene wave conditions and wave-induced sand transport in the southern North Sea. *Cont. Shelf Res.*, **21**(16–17), 1723–1749.

Van der Molen, J. and **de Swart, H.E.** (2001b) Holocene tidal conditions and tide-induced sand transport in the southern North Sea. *J. Geophys. Res.*, **106**(5), 9339–9362.

Van der Spek, A.J.F. (1995) Reconstruction of tidal inlet and channel dimensions in the Frisian Middelzee, a former tidal basin in the Dutch Wadden Sea. Tidal Signatures in Modern and Ancient Sediments. *Internat. Assoc. Sedimentol., Spec. Public.*, **24**, 239–258.

Van der Valk, L. (1995) *Toelichting bij de bladen 's-Gravenhage West (30W) en 's-Gravenhage Oost (30O).* Unpublished report, Rijks Geologische Dienst, Haarlem.

Van der Werf, K.M. (2020) *Tidal Peatlands: A Diatom Study in the Old Rhine Estuary, The Netherlands, Revealing the Role of Reed Peat in mid-Holocene Landscape Transitions.* MSc thesis. Utrecht University, Utrecht.

Van der Werff, A. and **Huls, H.** (1974) *Diatomeeënflora van Nederland*, pp. 1957–1974. Westzijde 13a.

Van der Woude, J.D. (1984) The fluviolagonal palaeoenvironment in the Rhine/Meuse deltaic plain. *Sedimentology*, **31**, 395–400.

Van Dinter, M. (2013) The Roman Limes in the Netherlands: How a delta landscape determined the location of the military structures. *Geologie en Mijnbouw/Neth. J. Geosci.*, **92**(1), 11–32.

Van Dinter, M., **Cohen, K.M.**, **Hoek, W.Z.**, **Stouthamer, E.**, **Jansma, E.** and **Middelkoop, H.** (2017) Late Holocene lowland fluvial archives and geoarchaeology: Utrecht's case study of Rhine river abandonment under Roman and Medieval settlement. *Quatern. Sci. Rev.*, **166**, 227–265.

Van Heeringen, R. and **Van der Valk, L.** (1989) *De mond van de Oude Rijn komt in beweging: IJzertijdvondsten uit het Katwijkse duingebied*, pp. 198–203. Westerheem, Amersfoort.

Van Kessel, T., **Spruyt-de Boer, A.**, **Van der Werf, J.**, **Sittoni, L.**, **Van Pooijen, B.** and **Winterwerp, H.** (2012). *Bed module for sand-mud mixtures.* Deltares, Delft, The Netherlands.

Van Lanen, R.J. and **Kosian, M.C.** (2020) What wetlands can teach us: reconstructing historical water-management systems and their present-day importance through GIScience. *Water History*, **12**(2), 151–177.

Van Oorschot, M., Kleinhans, M.G., Geerling, G., Egger, G., Leuven, R. and Middelkoop, H. (2017) Modeling invasive alien plant species in river systems: Interaction with native ecosystem engineers and effects on hydro-morphodynamic processes. *Water Resour. Res.*, **53**(8), 6945–6969.

Vermeer-Louman, G.G. (1934) Pollen-analytisch onderzoek van den West Nederlandschen bodem.

Vos, P.C. (2015) *Origin of the Dutch Coastal Landscape - Long-Term Landscape Evolution of the Netherlands During the Holocene Described and Visualized in National, Regional and Local Palaeogeographical Map Series*. Barkhuis, Groningen.

Vos, P.C., de Koning, J. and van Eerden, R. (2015) Landscape history of the Oer-IJ tidal system, Noord-Holland (The Netherlands). *Neth. J. Geosci.*, **94**(4), 295–332.

Vos, P.C. and De Wolf, H. (1988) Methodological aspects of palaeo-ecological diatom research in coastal areas of the Netherlands. *Geologie en Mijnbouw*, **67**, 31–40.

Vos, P.C. and De Wolf, H. (1993) Diatoms as a tool for reconstructing sedimentary environments in coastal wetlands; methodological aspects. *Hydrobiologica*, **269** (270), 285–296.

Vos, P.C. and Van Kesteren, W. (2000) The long-term evolution of intertidal mudflats in the northern Netherlands during the Holocene; natural and anthropogenic processes. *Cont. Shelf Res.*, **20**, 1687–1710.

Walker, M.J.C., Bell, M., Caseldine, A.E., Cameron, N.G., Hunter, K.L., James, J.H. and Johnson, S. (1998) Palaeoecological investigations of middle and late Flandrian buried peats on the Caldicot Levels, Severn Estuary, South Wales. *Proc. Geol. Assoc.*, **109**, 51–78.

Waller, M.P. (1994) Flandrian vegetational history of south-eastern England. Stratigraphy of the Brede valley and pollen data from Brede Bridge. *New Phytol.*, **126**, 369–392.

Waller, M.P. and Early, R. (2015) Vegetation dynamics from a coastal peatland: insights from combined plant macrofossil and pollen data. *J. Quatern. Sci.*, **30**, 779–789.

Waller, M.P. and Grant, M.J. (2012) Holocene pollen assemblages from coastal wetlands: differentiating natural and anthropogenic causes of change in the Thames estuary, UK. *J. Quatern. Sci.*, **27**, 461–474.

Waller, M.P. and Hamilton, S. (2000) The vegetation history of the English chalkland: a mid-Holocene pollen sequence from the Caburn, East Sussex. *J. Quatern. Sci.*, **15**, 253–272.

Waller, M. and Kirby, J. (2021) Coastal peat-beds and peatlands of the southern North Sea: their past, present and future. *Biol. Rev.*, **96**(2), 408–432.

Wang, Z., Saito, Y., Zhan, Q., Nian, X., Pan, D., Wang, L., Chen, T., Xie, J., Li, X. and Jiang, X. (2018) Three-dimensional evolution of the Yangtze River mouth, China during the Holocene: impacts of sea level, climate and human activity. *Earth-Sci. Rev.*, **185**, 938–955.

Warnock, J.P., Bauersachs, T., Kotthoff, U., Brandt, H.-T. and Andrén, E. (2018) Holocene environmental history of the Ångermanälven Estuary, northern Baltic Sea. *Boreas*, **47**, 593–608.

Wartenberg, W., Vött, A., Freund, H., Hadler, H., Frechen, M., Willershäuser, T., Schnaidt, S., Fischer, P. and Obrocki, L. (2013) Evidence of isochronic transgressive surfaces within the Jade Bay tidal flat area, southern German North Sea coast– Holocene event horizons of regional interest. *Zeitschrift für Geomorphologie – Suppl. Issues*, **57**, 229–256.

Weeda, E.J., Westra, R., Westra, C. and Westra, T. (1991) *Nederlandse oecologische Flora: Wilde planten en hun relaties 4*. IVN, Amsterdam, 315 p.

Weerts, H.J.T., Westerhoff, W.E., Cleveringa, P., Bierkens, M.F.P., Veldkamp, J.G. and Rijsdijk, K.F. (2005) Quaternary geological mapping of the lowlands of The Netherlands, a 21st century perspective. *Quat. Int.*, **133**, 159–178.

Weisner, S.E. (1987) The relation between wave exposure and distribution of emergent vegetation in a eutrophic lake. *Freshwat. Biol.*, **18**(3), 537–544.

Weisner, S.E. (1991) Emergent vegetation in Eutrophic Lakes: Distributional patterns and ecophysiological constraints.

Supporting Information

Additional information may be found in the online version of this article:

Appendix S1 Pierik *et al.* 'Vegetation composition and peat accumulation steer Holocene tidal-fluvial basin filling and overbank sedimentation along the Old Rhine River, The Netherlands'.

Appendix S2 Image gallery of a variety of diatom species encountered in cores *GW* and *BW*.